



universität  
wien

# DIPLOMARBEIT

Titel der Diplomarbeit

„Gas evolution from Lithium ion batteries studied in-situ by  
coupled GC/MS-FTIR“

verfasst von

Alfred Amon, BSc

angestrebter akademischer Grad

Diplom-Ingenieur (DI)

Wien, 2014

Studienkennzahl lt. Studienblatt:

A 066 658

Studienrichtung lt. Studienblatt:

Masterstudium >Chemie und Technologie der Materialien<

Betreut von:

Ao.Prof. Dr. Egon Erwin Rosenberg



# Acknowledgements

This work was financially supported by the Austrian Research Promotion Agency (FFG) within the scope of the *SiLithium* project (835790).

I am grateful to my mother and my father as well as my aunt and uncle who supported me during my whole life and my studies both mentally and financially and who made it possible for me to focus on my studies. Further I want to thank my girlfriend for her emotional support and patience.

I am much obliged to my supervisors Professor Erwin Rosenberg and Professor Atanaska Trifonova for their support and guidance and the possibility to conduct this thesis. Furthermore I want to thank my colleagues at the Vienna University of Technology and the Austrian Institute of Technology for their support and fruitful discussions, where especially Chrysoula Kanakaki, Zoltan Fekete, Raad Hamid, Irina Gocheva, Hristina Vasilchina, Arlavinda Rezquita, Joong-Hee Han and Katja Fröhlich provided valuable input and assistance.

I am also grateful for the excellent collaboration with the project partners from the companies *Shimadzu* (Korneuburg) and *i-RED* (Linz), where Wolfgang Märzinger and Jakub Kowalski supported me with the evaluation of the infrared data.





# Contents

<b>Acknowledgements</b>	<b>iii</b>
<b>Contents</b>	<b>v</b>
<b>List of Figures</b>	<b>vii</b>
<b>List of Tables</b>	<b>ix</b>
<b>Abbreviations and Symbols</b>	<b>xi</b>
<b>1 Introduction</b>	<b>1</b>
1.1 Introduction and Motivation . . . . .	1
1.1.1 Timeline . . . . .	3
1.2 Chemistry of Lithium Ion Batteries . . . . .	3
1.2.1 Characteristic Parameters . . . . .	5
1.2.2 Battery Design . . . . .	6
1.2.3 Cathode Active Materials . . . . .	6
1.2.4 Anode Active Materials . . . . .	7
1.2.5 Separators and Current Collectors . . . . .	8
1.2.6 Electrolytes . . . . .	9
1.2.7 Electrolyte Additives . . . . .	12
1.2.8 Thermal Runaway and Safety Precautions . . . . .	12
1.3 Electrolyte decomposition and gas evolution . . . . .	14
1.3.1 Determination of the electrochemical stability . . . . .	14
1.3.2 Decomposition under oxidative conditions . . . . .	15
1.3.3 Decomposition under reductive conditions . . . . .	19
1.3.4 Thermally induced reactions . . . . .	22
1.3.5 Techniques for the analysis of evolved gases from lithium ion bat- teries . . . . .	24
1.4 Gas Chromatography / Mass Spectrometry . . . . .	25
1.5 Fourier Transform Infrared Spectroscopy . . . . .	26
<b>2 Experimental Part</b>	<b>27</b>
2.1 Materials . . . . .	27
2.1.1 Consumables . . . . .	27
2.1.2 Electrodes . . . . .	28
2.1.3 Boston Power – Swing 4400 . . . . .	28

2.2	Instruments . . . . .	29
2.2.1	Electrochemical Equipment . . . . .	29
2.2.2	GC/MS . . . . .	29
2.2.3	FTIR Spectrometer . . . . .	32
2.2.4	Gas Sampling Cells . . . . .	33
2.3	Development of the Gas Measurement Technique . . . . .	35
<b>3</b>	<b>Results and Discussion</b>	<b>39</b>
3.1	Preliminary Experiments . . . . .	39
3.1.1	Swing 4400 Electrolyte Composition . . . . .	40
3.2	In-situ Gas Measurements . . . . .	41
3.2.1	Gas evolution from the Swing 4400 cell . . . . .	41
3.2.1.1	Cycling in normal voltage range . . . . .	41
3.2.1.2	Overcharge . . . . .	42
3.2.2	Gas evolution from coin cells . . . . .	48
3.2.2.1	Glassy Carbon Electrodes . . . . .	49
3.2.2.2	Formation Pathways of the Compounds . . . . .	54
3.2.2.3	LiCoO <sub>2</sub> Electrodes . . . . .	55
<b>4</b>	<b>Conclusions</b>	<b>61</b>
	<b>Bibliography</b>	<b>63</b>
<b>A</b>	<b>Additional Figures</b>	<b>67</b>
<b>B</b>	<b>Abstract (English)</b>	<b>71</b>
<b>C</b>	<b>Abstract (German)</b>	<b>73</b>
<b>D</b>	<b>Curriculum Vitae</b>	<b>75</b>

# List of Figures

1.1	Timeline . . . . .	3
1.2	Scheme of an intercalation battery . . . . .	4
1.3	Construction schemes of cylindrical cells and coin cells . . . . .	6
1.4	Series of oligomeric decomposition products reported in literature. . . . .	20
2.1	Photograph and scheme of the 10-port sampling valve . . . . .	30
2.2	Photograph of the PTFE gas sampling cell . . . . .	33
2.3	Assembly of the coin cell gas sampling setup . . . . .	34
2.4	Cross section of the coin cell gas sampling cell . . . . .	35
2.5	Scheme of the In-situ gas analysis setup . . . . .	37
2.6	Photograph of the In-situ gas analysis setup . . . . .	37
2.7	Photograph of the In-situ gas analysis setup in detail . . . . .	38
3.1	Cycling program: Preliminary experiments . . . . .	39
3.2	Mass spectra of compounds found during normal cycling of the BPC . . .	42
3.3	Mass spectrum of methyl acetate . . . . .	43
3.4	CO <sub>2</sub> signal during the overcharge of the BPC. . . . .	43
3.5	Mass spectra of unidentified compounds from the BPC . . . . .	44
3.6	Gas chromatogram of the compounds evolved from the BPC. Recorded at a charging voltage of 4.75 V . . . . .	46
3.7	Development of the charging voltage and cell temperature (smoothed) during the overcharge of the BPC. The steps in the temperature curve result from the temperature resolution of 1 °C of the digital thermometer. .	47
3.8	GC/MS and FTIR signals during the BPC overcharge . . . . .	48
3.9	FTIR signal for the evolution of several gaseous compounds during the BPC overcharge. . . . .	49
3.10	Cyclic voltammogram for DMC, EC and DMC/EC on glassy carbon . . .	52
3.11	CO <sub>2</sub> signal recorded during the cyclic voltammetry of DMC, EC and DMC/EC on glassy carbon. . . . .	52
3.12	GC/MS signals for several gases during the cyclic voltammetry of DMC on a glassy carbon electrode. . . . .	53
3.13	Gas chromatogram recorded at a potential of 6.92 V from DMC on a glassy carbon electrode. . . . .	53
3.14	Mass spectra of unidentified compounds from DMC decomposition on a glassy carbon electrode. . . . .	54
3.15	Cyclic voltammetry curves of DMC/EC with GC- and LiCoO <sub>2</sub> working electrodes . . . . .	57
3.16	Cyclic voltammetry curve and gas evolution of DMC/EC on LiCoO <sub>2</sub> . . .	57
3.17	Gas chromatograms of DMC/EC on glassy carbon and LiCoO <sub>2</sub> . . . . .	59

A.1	Cyclic voltammetry curve and gas evolution of DMC/EC on $\text{LiCoO}_2$ . . .	67
A.2	Gas chromatogram recorded from the BPC in the normal charging voltage range. . . . .	68
A.3	Gas chromatogram recorded during the overcharge of the BPC. . . . .	68
A.4	Gas chromatogram recorded during the cyclic voltammetry of EC on glassy carbon . . . . .	69
A.5	Charging voltage and temperature during BPC overcharge . . . . .	69

# List of Tables

1.1	Physical properties of organic solvents . . . . .	11
1.2	Properties of Li salts . . . . .	12
1.3	Electrochemical stability of solvents . . . . .	13
2.1	Specifications of chromatography columns used. . . . .	31
2.2	GC/MS parameters of method A . . . . .	31
2.3	GC/MS parameters of method B . . . . .	31
2.4	GC/MS parameters of method C . . . . .	32
3.1	Compounds identified from the separators cycled during preliminary experiments . . . . .	40
3.2	Compounds identified by GC/MS in the electrolyte of the Swing 4400 cell. . . . .	41
3.3	Compounds identified during the overcharge of the BPC with the Rtx-5MS column . . . . .	44
3.4	Compounds identified during the overcharge of the BPC with the PLOT column . . . . .	45
3.5	Compounds identified by GC/MS during cyclic voltammetry of LiPF <sub>6</sub> in DMC, EC and DMC/EC . . . . .	51
3.6	Compounds assigned to their suspected formation mechanism . . . . .	55
3.7	Compounds identified by GC/MS during cyclic voltammetry of LiPF <sub>6</sub> in DMC/EC on glassy carbon and LiCoO <sub>2</sub> electrodes . . . . .	58



# Abbreviations and Symbols

Abbreviation or Symbol	
<b>BPC</b>	Boston Power Cell <i>Swing 4400</i>
<b>cP</b>	Centipoise (1 cP = 1 mPa s)
<b>DEC</b>	Diethyl carbonate
<b>DMC</b>	Dimethyl carbonate
<b>EC</b>	Ethylene carbonate
<b>EMC</b>	Ethyl methyl carbonate
<b><i>E<sub>OC</sub></i></b>	Open-circuit Voltage
<b>F</b>	Faraday constant (F = 96485.3 C/mol)
<b>FTIR</b>	Fourier transform infrared spectrometry
<b><i>G<sub>m</sub></i></b>	Molar Gibbs Energy
<b>GC</b>	Glassy carbon
<b>GC/MS</b>	Gas chromatography/mass spectrometry
<b>LIB</b>	Lithium ion battery
<b>M</b>	molar (1 M = 1 mol/L)
<b>MeOLi</b>	Lithium methanolate
<b>mS</b>	milli Siemens (1 S=1 A/V)
<b>MW</b>	Molar weight (unit: g/mol)
<b>PC</b>	Propylene carbonate
<b>PLOT</b>	Porous layer open tubular column
<b>PLS</b>	Partial Least Squares
<b>RT</b>	Retention time
<b>SEI</b>	Solid-electrolyte-interface (also: interphase)
<b>z</b>	Number of electrons transferred in the reaction
<b><math>\mu</math></b>	Chemical potential





# Chapter 1

## Introduction

### 1.1 Introduction and Motivation

Our daily life is governed by modern electronic devices and an increasing demand for mobility. One of the main concerns of engineers and researchers is therefore to improve our possibility to store and provide electrical energy wherever it is needed. The invention of batteries made it possible to develop mobile phones, pacemakers, digital cameras, electric vehicles and many other devices which depend on mobile power supply. Rechargeable batteries, also termed secondary cells, have been developed over decades to give higher voltages and capacities as well as improved cyclability. For mobile applications the gravimetric capacity, i.e. capacity per weight, is especially important and numerous efforts have been made to find lightweight materials with high capacities.

In modern devices the lithium ion battery (LIB) has become the most important rechargeable battery type. It exceeds because of its high cell voltage, high gravimetric capacity and excellent rechargeability. The development began in the 1970's when the  $\text{Li}_x\text{TiS}_2$ -phase was discovered as a possible intercalation cathode material [1, 2]. Since then various cathode materials have been developed to achieve higher cell voltage and capacity, where the most successful are  $\text{LiFePO}_4$  and transition metal oxides based on  $\text{LiCoO}_2$  or  $\text{LiMn}_2\text{O}_4$ .

Although metallic lithium is a very appealing anode material due to its low standard potential and its low density, it shows poor cyclability because of dendritic Li-deposition during discharge. Only the discovery of graphite as a Li-intercalation anode [3, 4] enabled the construction of LIBs with acceptable cyclability and capacity. For the anode

side carbon based materials are still the most common but metal based anodes are in development. In 1990 the first commercial LIB was announced by Sony, Japan [1].

A major challenge, besides improved electrode materials, is to find electrolytes which are stable against oxidation and reduction at the working potentials of the battery electrodes. This stability region is often called the *electrochemical window* of the electrolyte. Especially the low potential of the anode excludes any protic solvents. The electrolyte should also have sufficient ionic conductivity and be inert towards the battery components. As later discovered, the reactivity of the electrolyte towards the graphite anode is of special importance, as it forms a protective layer, termed *solid electrolyte interface* (SEI), on the electrode which prevents further electrolyte decomposition [5]. Most electrolytes which are in successful commercial application for LIBs consist of Li-salts dissolved in a mixture of organic solvents, the most prominent being linear and cyclic organic carbonates and ethers. The improvement of electrolyte stability is a major issue concerning battery safety. The solvents used are usually highly flammable and in case of battery failure their highly exothermic combustion leads to the evolution of toxic and flammable gases. Especially the so-called *thermal runaway*, where a self accelerating reaction cascade can lead to explosions of the battery, was investigated intensely. Modern batteries have several built-in fail-safe systems to prevent accidents but safety on the chemical level is still the most important issue.

In the last years several reports about cellphone batteries and also batteries of electric cars involved in accidents catching fire became public news [6]. While the fires from cellphone batteries usually stay under control, the large battery packs in electric vehicles can pose a dangerous threat. To ensure the success of electric vehicles we have to improve the safety of LIBs and to better understand the processes which occur before and during battery failure.

The goal of this work is to develop a method for the in-situ characterisation of gaseous emissions from LIBs. For this purpose a device for the collection of the evolved gases from a LIB during the charging procedure was connected to a gas chromatography/mass spectrometry instrument (GC/MS). Later the setup was completed by connecting a Fourier Transform Infrared Spectrometer (FTIR) for simultaneous measurement. This configuration combines the complimentary features of both instruments. GC/MS is suited for the identification and quantification of complicated analyte mixtures over a wide range of concentrations. Unfortunately its time resolution is rather low since a measurement

takes typically between 10 and 20 minutes. FTIR lacks the low detection limit and the ability to distinguish complicated mixtures but its temporal resolution is in comparison only limited by the desired spectral resolution. A partial least squares regression (PLS) correlates the FTIR signal with the GC/MS data and allows the quantification of the FTIR signal.

With this, to our knowledge, unprecedented setup I examined the gas evolution from a commercial high power LIB as well as from coin cell type batteries. The coin cell approach allows the variation of the cell composition to investigate the influences from different electrolyte components and electrode material separately. A special challenge was the detection of the small amounts of gases evolved from the coin cells.

### 1.1.1 Timeline

The practical aspects of this work have been conducted between 1<sup>st</sup> October 2013 and 30<sup>th</sup> May 2014 (Figure 1.1).

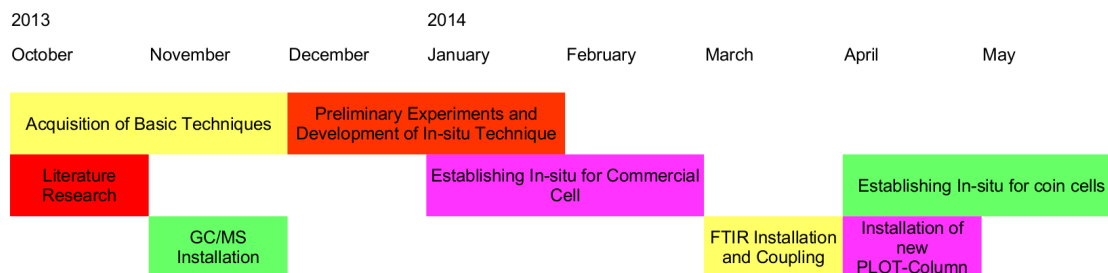


FIGURE 1.1: Approximate timeline of this thesis.

## 1.2 Chemistry of Lithium Ion Batteries

State of the art LIBs are constructed by the so-called *rocking-chair* principle. In contrast to *Lithium Batteries* which contain a metallic Lithium anode, in *Lithium Ion Batteries* both electrodes are comprised of Li-intercalation compounds. During charge and discharge Li ions are moving from the cathode to the anode and vice versa. On the anode side graphite is the most common material, while transition metal oxides are used for the cathode. By applying an external voltage to the electrodes the electrode potentials are shifted and lithium ions are extracted from the cathode material and intercalated in the anode active material, while electrons flow through the outer electrical circuit to

maintain charge balance (Figure 1.2) [7]. The transition metal ion (M) in the cathode materials is oxidised during this reaction (1.1) and the graphite is reduced (1.2). The Gibbs energy change  $\Delta G$  of this reaction is positive thus work has to be performed on the system. During discharge the reverse reaction takes place which has  $\Delta G < 0$  and therefore can perform electrical work on an external circuit, hence work as a battery. The overall cell reaction is given by equation (1.3).

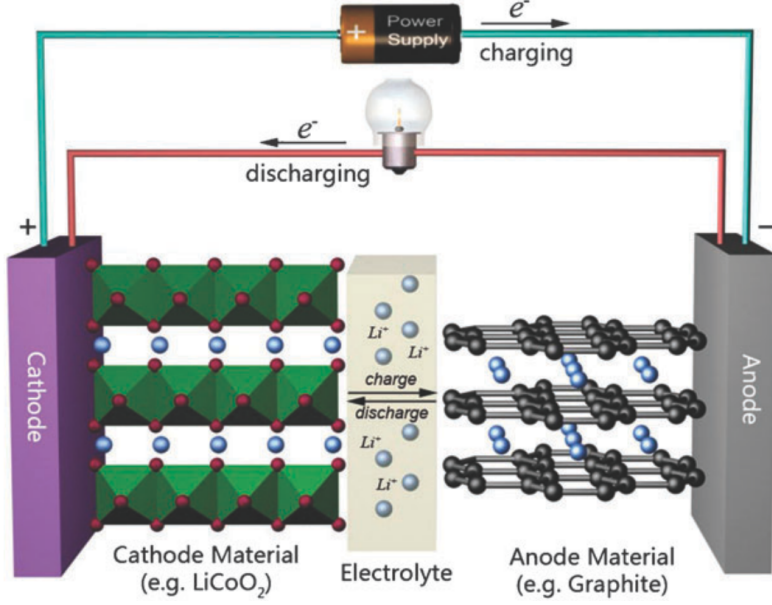
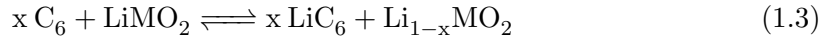


FIGURE 1.2: Scheme of the LIB operation mode, showing the de-/intercalation of Li (blue/grey spheres) in the electrodes. Figure retrieved from [8].



The open circuit voltage  $E_{OC}$  of a battery is directly related to the molar Gibbs energy change  $\Delta G_m$  of the cell reaction by equation (1.4), where  $z$  is the number of electrons transferred in the reaction and  $F$  Faraday's constant. This voltage corresponds to the difference of the chemical potentials of Li in the cathode  $\mu_{Li}^c$  and the anode  $\mu_{Li}^a$  (1.5)

which comprise the chemical potential of the  $\text{Li}^+$  ion and the electron (1.6, 1.7).

$$\Delta G_m = -zFE_{OC} \quad (1.4)$$

$$E_{OC} = -\frac{\mu_{Li}^c - \mu_{Li}^a}{zF} \quad (1.5)$$

$$\mu_{Li}^c = \mu_{Li+}^c + \mu_{e-}^c \quad (1.6)$$

$$\mu_{Li}^a = \mu_{Li+}^a + \mu_{e-}^a \quad (1.7)$$

The value of  $\mu_{Li+}$  depends mainly on the site energy of the  $\text{Li}^+$  ion in the intercalation materials and  $\mu_{e-}$  corresponds to the Fermi level [9]. The electronic and crystal structure of the host materials are therefore the properties which determine the achievable cell voltage. To obtain a high open circuit voltage  $E_{OC}$  a cathode with a low  $\mu_{Li}$  and an anode with a high  $\mu_{Li}$  are combined.

### 1.2.1 Characteristic Parameters

To characterise and compare the properties and performance of LIBs several parameters have been established. Some of the most important are:

**Nominal Voltage** The battery's reported voltage.

**Cut-off Voltage** The discharge voltage limit which is recommended for safe use of the battery [10].

**End-of-charge Voltage** The charging voltage limit which is recommended for safe use of the battery.

**Specific Capacity  $Q_{th}$**  The charge stored per g of battery mass or electrode mass.

$$Q_{th} = \frac{z \times F}{MW} \text{ mAh/g}$$

**Energy Density  $W_{th}$**  The energy stored per g of battery mass or electrode mass [10].

$$W_{th} = \frac{E \times z \times F}{MW} \text{ mWh/g}$$

**C-Rate** The charge/discharge current at which the battery would be charged/discharged within  $\frac{1}{C-rate}$  hours.

### 1.2.2 Battery Design

A battery is made of two electrodes which are electronically insulated from each other by a separator but in contact with an electrolyte that ensures ionic conductivity. The electrodes usually consist of a metal foil as current collector on which a composite material containing the active constituents is coated. This composite is prepared as a slurry from the active material powder, a carbon additive to enhance electronic conductivity and a binder like polyvinylidene fluoride that increases the mechanical stability. There are several popular cell geometries depending on the application of the battery (Figure 1.3). In coin cells, also known as button cells, the circular electrodes are stacked inside a metal cup which is then closed tightly by crimping a metal cap on top. These metal parts serve also as connecting leads. Coin cells are easy and cheap to assemble and typically used for non-rechargeable batteries. Cylindrical cells are made from long metal foil bands which are coated on both sides with active mass and serve as current collectors. The two electrodes are separated by a separator band and rolled up to a tight bundle which is inserted in a metal can. This design has good mechanical stability and the tight stacking of the electrodes provides a high capacity per volume.

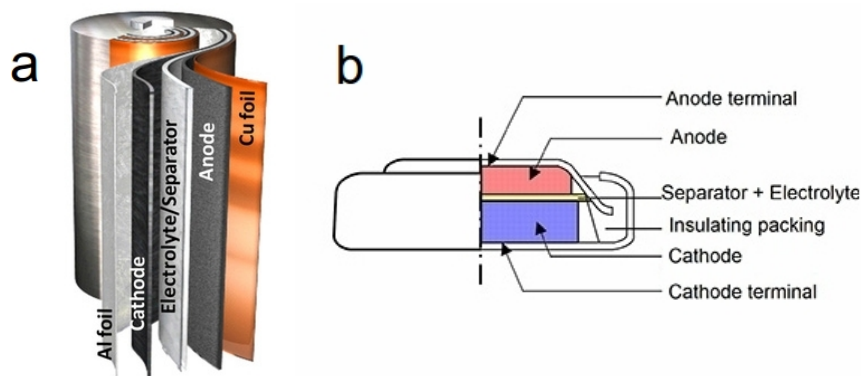
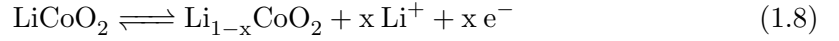


FIGURE 1.3: Construction schemes of (a) cylindrical cells and (b) coin cells. Reproduced from [11] and [12], respectively.

### 1.2.3 Cathode Active Materials

Cathode materials of widespread commercial use are  $\text{LiCoO}_2$ ,  $\text{LiMn}_2\text{O}_4$  and  $\text{LiFePO}_4$ .  $\text{Li}_{1-x}\text{CoO}_2$  was used in the first commercial LIB and has a theoretical capacity of 274 mAh/g with an average voltage of 3.9 V versus  $\text{Li}/\text{Li}^+$ . Yet the practical capacity is merely around 130 mAh/g because only about 50 % of the contained Li can be extracted

reversibly (1.8). Overcharging beyond 4.2 V can lead to structural instability and the material becomes prone to the release of oxygen (1.9) which can react with the electrolyte [1, 13].  $\text{LiCoO}_2$  has a hexagonal crystal structure which consists of alternating layers of Co and Li ions which are octahedrally coordinated by oxygen. The toxicity and high price of Cobalt are the main drawbacks of this cathode material. Layered structures containing also Ni, Mn and Al have been developed with improved capacity and stability [14].



**$\text{Li}_{1-x}\text{Mn}_2\text{O}_4$**  shows a higher nominal voltage than  $\text{LiCoO}_2$  but its practical capacity is only around 100 - 120 mAh/g.  $\text{Li}^+$  ions can be intercalated in the tetrahedral (1.10) and octahedral sites of the spinel structure, but only the former ones give the high voltage of 4.1 V. The excellent high rate performance and the availability and low toxicity of manganese make up for the low capacity [14]. Problems are associated with self-discharge due to  $\text{Mn}^{2+}$  dissolution in the electrolyte and also oxygen release, although at higher voltages than  $\text{LiCoO}_2$  [15].



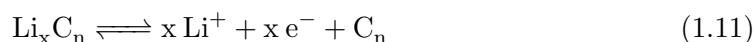
**$\text{LiFePO}_4$**  is also a low cost and low toxicity material. Its excellent high rate performance makes it popular for power tools. In contrast to  $\text{Li}_{1-x}\text{CoO}_2$  and  $\text{Li}_{1-x}\text{Mn}_2\text{O}_4$ , in which  $\text{Li}^+$  is intercalated gradually, a phase transition from  $\text{FePO}_4$  to the olivine structure  $\text{LiFePO}_4$  occurs upon  $\text{Li}^+$  insertion. It provides a stable discharge voltage of 3.45 V. With a theoretical specific capacity of 170 mAh/g and a high stability against oxygen release the low electronic conductivity is its main disadvantage [14].

#### 1.2.4 Anode Active Materials

**Metallic Lithium** would be an excellent anode material due to its low standard potential ( $E^\circ = -3.045 \text{ V}$  vs. standard hydrogen electrode) and its low density ( $\delta = 0.534 \text{ g/cm}^3$ ) [16]. Unfortunately Li is forming dendrites during redeposition on

the anode side. This causes internal short circuits due to dendrites growing through the separator and also reduces the capacity when the dendrites break and lose electrical contact with the anode. Hence metallic lithium anodes are mainly used in non-rechargeable cells [17].

**Graphitic carbons** are the prevalent anode materials in commercial cells. On charging lithium ions are intercalated between the layers over several steps up to  $\text{LiC}_6$  (1.11). The potential vs.  $\text{Li}/\text{Li}^+$  ranges from  $\sim 0.8\text{ V}$  (for  $x < 0.1$  in  $\text{Li}_x\text{C}_6$ ) to  $\sim 0.1\text{ V}$  ( $x = 1$ ) with a theoretical capacity of  $372\text{ mAh/g}$  [18].



The low potential of the graphite anode leads to the reduction of solvent species and the formation of a passivation layer on the surface during the first charging cycle. This layer was termed *solid electrolyte interface* (SEI) as it is an ionic conductor but an electronic insulator thus allowing the diffusion of  $\text{Li}^+$  to the graphite but preventing the further reduction of the electrolyte. It forms around  $0.8\text{--}2\text{ V}$  and has a complex composition of inorganic and organic decomposition products like  $\text{Li}_2\text{CO}_3$ , Li alkyl carbonates and polymerisation products of the electrolyte [19].

**Intermetallic anodes** are very promising for future batteries as they have theoretical capacities which are a multiple of graphite. The most promising amongst them is silicon which has a theoretical capacity over  $4000\text{ mAh/g}$ . The huge volume change upon lithiation is still troubling though and prevents a capacity retention over many cycles [20].

### 1.2.5 Separators and Current Collectors

To avoid an internal short circuit the electrodes are separated from each other by an ion conducting membrane. The separator should have high mechanical, thermal and chemical stability and provide sufficient conductivity for the Li salt while being electronically insulating. It should be able to retain the electrolyte solution without swelling. Separators made of porous polyethylene or polypropylene sheets, which are soaked with electrolyte, are popular in commercial LIBs. They are usually designed with a so-called



*shut-down-fail* safe mechanism. If the temperature in the battery exceeds a certain threshold, usually around 130 °C, the pores of the membrane close and interrupt the internal current flow [21]. Current collectors made of copper and aluminium foil are used for the anode and cathode side, respectively. The stability of Al at high potentials was explained by the formation of Al halide layers which passivate the surface against dissolution [22].

### 1.2.6 Electrolytes

Commercial liquid electrolytes for LIBs, omitting polymeric electrolytes and solid electrolytes, consist of a Li salt dissolved in a mixture of organic solvents. A suitable solvent requires a range of properties which are often hard to achieve by a single component and reasonable compromises have to be made [5]. Protic solvents are inapplicable as they are not stable against reduction at the anode leading to decomposition and H<sub>2</sub> evolution. The following criteria have to be considered during the design of a LIB electrolyte:

**Liquid Range** The temperature range between the liquidus temperature and the boiling point of the electrolyte.

**Viscosity** Low viscosity increases the ionic conductivity but comes often only with low polarity of the solvent.

**Permittivity** Polar solvents show good solubility for the Li salts used and enable high concentrations.

**Ionic conductivity** It depends on the concentration and mobility of charge carriers, i.e. ions, in the solvent.

**Electrochemical Window** The electrolyte components should be stable, thermodynamically or kinetically, against oxidation or reduction at the electrodes.

**Thermal stability** The components should not decompose at the working or storage temperatures of the battery.

**Toxicity** Highly toxic substances should be avoided.

**Flammability** To avoid fires or explosions in cases of battery failure low flammability is desirable.

As can be seen from the values given in Table 1.1 solvents with high relative permittivity, i.e. high polarity, often have high melting points and are rather viscous, while solvents of low viscosity have low permittivity which goes with low salt solubility. Practical electrolytes are therefore a mixture of low and high polarity solvents.

Cyclic ethers were found to be resistant against reduction but are oxidised at Pt-electrodes around 4.0 V and at real cathode materials at even lower potentials. Cyclic carbonates like ethylene carbonate (EC) and propylene carbonate (PC) show stability against oxidation up to 5 V and are stable towards the anode due to SEI-formation. PC is well established with metallic Li anodes but is incompatible with graphite anodes. It was found that the PC molecules intercalate in the graphite leading to destruction of the layered structure by *exfoliation* [5]. EC on the contrary forms stable SEIs with good ionic conductivity. To improve the low temperature behaviour of EC it is used in a mixture with linear carbonates like dimethyl carbonate (DMC) [23]. This lowers the solidification temperature and viscosity with only a small trade-off in polarity.

Several Li salts have been examined for the electrolyte but up to now  $\text{LiPF}_6$  has proven to be the most suitable. The salt should be highly soluble in the used solvent, show high ion mobility and the anion has to be inert against the electrodes and the solvent itself. This rules out most candidates like Li halides which are either not soluble enough in organic solvents or easily oxidised at the cathode. Salts based on Lewis acids are prevalent in commercial LIBs. The anions can be seen as Lewis acids e.g.  $\text{PF}_5$  which are complexed by a Lewis base like  $\text{F}^-$  (1.12).



While Al based anions are too reactive and cause corrosion in the cell, milder Lewis acids like  $\text{LiBF}_4$ ,  $\text{LiPF}_6$ ,  $\text{LiAsF}_6$  and  $\text{LiClO}_4$  have been investigated for their use in LIBs.

**$\text{LiClO}_4$**  shows high conductivity and high anodic stability. Also the SEI formed with  $\text{LiClO}_4$  was found to have especially low resistance as no HF is generated. Its strong oxidation power causes high reactivity with the solvent and it is only used in laboratory applications due to its low price and easy handling.

**$\text{LiAsF}_6$**  is like  $\text{LiClO}_4$  stable at high potentials and rather resistant against hydrolysis. A cathodic reaction resulting in the formation of the highly toxic  $\text{AsF}_3$  gas excluded this salt from commercial use.

**$\text{LiBF}_4$**  finds new popularity as a replacement for the thermally unstable  $\text{LiPF}_6$  while

mainly its moderate conductivity, due to the low dissociation constant, prevents its advance.

**LiPF<sub>6</sub>** is the prevalent salt in commercial electrolytes. Although it does not outperform the other candidates in their particular properties, it has the best balance of all required features. The biggest drawbacks are the high sensitivity towards moisture and the low stability against thermal decomposition. The equilibrium of reaction (1.13) is shifted to the right side due to the formation of the gas PF<sub>5</sub> which begins at rather low temperatures (cf. Table 1.2). This also interferes with the ability to dry the salt. Solvents which show high solubility mitigate reaction (1.13) since the rate depends on the concentration of the undissociated LiPF<sub>6</sub> species. Already small amounts of water cause the formation of corrosive products (1.14, 1.15) which attack the organic solvent and decrease battery life. The production of high purity salts with low water content has been crucial to the success of LiPF<sub>6</sub> [5].

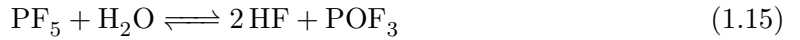
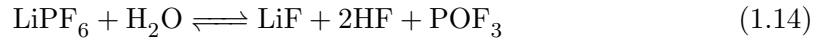
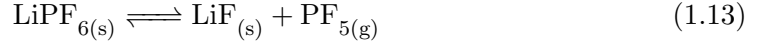


TABLE 1.1: Physical properties of solvents at 25°C (unless noted). From ref. [5, 24].

Solvent	Melting Point	Boiling Point	Rel. Permittivity	Viscosity
Ethylene-carbonate	36.4°C	248°C	89.78 (40°C)	1.9 cP (40°C)
Dimethyl-carbonate	4.6°C	91°C	3.11	0.59 cP (20°C)
Diethyl-carbonate	-74.3°C	126°C	2.81 (20°C)	0.75 cP
Ethylmethyl-carbonate	-53°C	110°C	2.96 (20°C)	0.65 cP
Propylene-carbonate	-48.8°C	242°C	64.92	2.53 cP
Diethylether	-116.3°C	34.55°C	4.23	0.242 cP
Dimethoxy-ethane	-58°C	84°C	7.2	0.46 cP
Tetrahydrofuran	-108.5°C	65.97°C	7.43	0.459 cP

Typical commercial electrolytes are a mixture of several solvents like DMC, EC, EMC, DEC or PC where a good balance between conductivity, thermal properties, stability and SEI formation has to be found. As a salt LiPF<sub>6</sub> is used typically with concentrations

TABLE 1.2: Properties of common Li salts. Collected from ref. [5]

Salt	T <sub>Decomp, solv.</sub>	Al-corrosion	Conductivity (1.0 M, EC/DMC, 25 °C )
LiClO <sub>4</sub>	>100 °C	No	8.4 mS/cm
LiAsF <sub>6</sub>	>100 °C	No	11.1 mS/cm
LiBF <sub>4</sub>	>100 °C	No	4.9 mS/cm
LiPF <sub>6</sub>	>100 °C	No	10.7 mS/cm

of 1 mol/L. Standard electrolytes for R&D are *LP 30* (DMC/EC 1:1 by weight, 1 M LiPF<sub>6</sub>) or *LP 40* (DEC/EC 1:1 by weight, 1 M LiPF<sub>6</sub>).

### 1.2.7 Electrolyte Additives

Do mitigate the deficits of the electrolytes, additives have been investigated to improve the properties of the anode passivation layer (SEI), for cathode protection, overcharge protection as well as wetting agents and flame retardants.

Vinyliden carbonate (VC) greatly improves the properties of the anode passivation layer. It even enables the use of PC as electrolyte. The lowest unoccupied molecular orbital of VC is of lower energy than for other solvents due to the double bond. It is reduced at higher potentials than the solvent, forms the SEI and avoids the reduction of EC and gas evolution. Also S-containing compounds like ethylene sulfite, propylene sulfite and diethyl sulfite have been investigated as SEI forming additives [30]. Biphenyl was found to act as a overcharge preventing additive as it polymerises on the cathode surface around 4.75 V forming an isolating film [31].

### 1.2.8 Thermal Runaway and Safety Precautions

If the temperature inside the battery is too high, due to wrong charging or other influences, a cascade of self-accelerating reactions can start along with extreme heat evolution. This was named a *thermal runaway*. In the worst case this leads to the ignition or explosion of the battery. The initiation is suspected to originate from the destabilisation of the SEI film at the anode and subsequent direct reaction of the electrolyte with the anode. This was observed at temperatures below 100 °C. The transition metal oxides are also prone to release oxygen at higher temperatures which fuels the reactions. Most

TABLE 1.3: Electrochemical stability of solvents. Collected from references [25–29].  
AC: Activated Carbon. GC: Glassy Carbon

Solvent	Salt	Working electrode	Anodic Limit	Cathodic Limit
DMC	LiClO <sub>4</sub>	Au		1.32 V [25]
	LiClO <sub>4</sub>	GC	5.7 V	[26]
	LiPF <sub>6</sub>	GC	~ 6.3 V	[27]
	LiPF <sub>6</sub>	LiMn <sub>2</sub> O <sub>4</sub>	~ 4.2 V	[27]
DEC	LiClO <sub>4</sub>	Au		1.32 V [25]
	LiClO <sub>4</sub>	GC	5.5 V	[26]
EMC	LiPF <sub>6</sub>	GC	~ 6.7 V	[27]
	LiPF <sub>6</sub>	LiMn <sub>2</sub> O <sub>4</sub>	~ 4.5 V	[27]
EC	LiClO <sub>4</sub>	Au		1.36 V [25]
	Et <sub>3</sub> MeN <sup>+</sup> PF <sub>6</sub> <sup>−</sup>	GC	6.70 V	0.11 V [27]
	Et <sub>3</sub> MeN <sup>+</sup> PF <sub>6</sub> <sup>−</sup>	AC	4.60 V	1.94 V [27]
PC	LiClO <sub>4</sub>	Au		1.0–1.6 V [25]
	Et <sub>3</sub> MeN <sup>+</sup> PF <sub>6</sub> <sup>−</sup>	GC	5.98 V	0.23 V [27]
	Et <sub>3</sub> MeN <sup>+</sup> PF <sub>6</sub> <sup>−</sup>	AC	4.42 V	2.25 V [27]
	LiClO <sub>4</sub>	GC	5.8 V	[26]
	LiClO <sub>4</sub>	GC	5.3 V	[28]
	LiClO <sub>4</sub>	Pt	5.3 V	[28]
VC	LiClO <sub>4</sub>	Au		1.40 V [25]
EC/DMC	Et <sub>3</sub> MeN <sup>+</sup> PF <sub>6</sub> <sup>−</sup>	GC	6.69 V	0.15 V [27]
	Et <sub>3</sub> MeN <sup>+</sup> PF <sub>6</sub> <sup>−</sup>	AC	4.52 V	2.03 V [27]
	LiPF <sub>6</sub>	LiMn <sub>2</sub> O <sub>4</sub>	~ 6.0 V	[27]
	LiPF <sub>6</sub>	Pt	~ 6.5 V	[27]
	LiPF <sub>6</sub>	GC	~ 6.5 V	[27]
	LiPF <sub>6</sub>	Au	3.55 V	[29]
	LiPF <sub>6</sub>	Pt	3.45 V	[29]
	LiPF <sub>6</sub>	Al	3.3 V	[29]
	LiAsF <sub>6</sub>	Au	3.55 V	[29]
	LiAsF <sub>6</sub>	Al	3.4 V	[29]
PC/DMC	Et <sub>3</sub> MeN <sup>+</sup> PF <sub>6</sub> <sup>−</sup>	GC	5.78 V	0.18 V [27]
	Et <sub>3</sub> MeN <sup>+</sup> PF <sub>6</sub> <sup>−</sup>	AC	4.10 V	2.20 V [27]
EC/EMC	Et <sub>3</sub> MeN <sup>+</sup> PF <sub>6</sub> <sup>−</sup>	GC	6.68 V	0.10 V [27]
	Et <sub>3</sub> MeN <sup>+</sup> PF <sub>6</sub> <sup>−</sup>	AC	4.58 V	2.06 V [27]
PC/EMC	Et <sub>3</sub> MeN <sup>+</sup> PF <sub>6</sub> <sup>−</sup>	GC	6.20 V	0.11 V [27]
	Et <sub>3</sub> MeN <sup>+</sup> PF <sub>6</sub> <sup>−</sup>	AC	4.24 V	2.03 V [27]
EC/PC	LiClO <sub>4</sub>	GC	5.8 V	[26]

of these reactions lead to gas evolution and an internal pressure build up in the cell. If the pressure gets too high the battery explodes and vents the hot flammable gases were they can react with the atmospheric oxygen. The main energy contribution of these reactions is the combustion of the organic electrolyte [32].

Batteries contain several non-chemical safety features that come into play to avoid battery failure:

**PTC** A positive temperature coefficient switch which increases its resistance above a certain temperature to disrupt the circuit.

**CID** Circuit interrupt devices which interrupt the electrical circuit if the internal pressure is too high.

**Safety vents** which open to release evolved gases in a controlled way.

**BMS** The battery management system monitors temperature and charging state of the battery amongst other parameters. It controls the charging and discharging processes and intervenes in the event of a failure.

## 1.3 Electrolyte decomposition and gas evolution

### 1.3.1 Determination of the electrochemical stability

The electrolyte stability problem is known in the field of LIBs since the introduction of the lithium metal anode. Many scientists have investigated the stability regions of common electrolytes but the literature data are sometimes ambiguous or contradictory and different values have been published for the same system. This is mainly due to the fact that the electrolyte stability limit depends on many factors. The type and concentration of the salt, the level of impurities and the working electrode material have been found to influence the onset potential of decomposition reactions tremendously — compare Table 1.3. Also the experimental approach to these values accounts for their large variations. Although it was stated by many authors that electrolyte stability limits should be evaluated at actual LIB electrodes only few authors have reported such values [27]. The onset potential is usually determined by cyclic voltammetry (CV) and differences in the data evaluation give rise to values which can be hard to compare. In

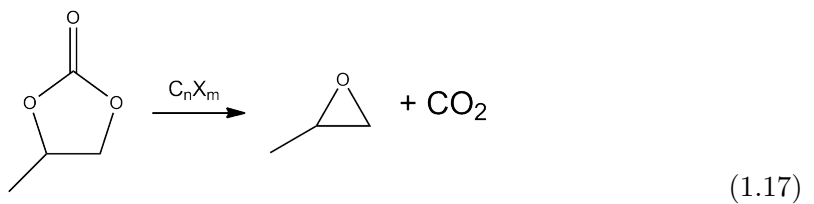
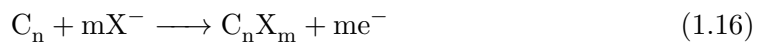
some papers [26, 29], the onset of the decomposition reaction is given by the intersection of two tangents at the  $i = 0$  base line and the slope of the peak. As elaborated in ref.[33] this intersection can change strongly with the choice of the current range. The second popular method is to define it as the potential where the measured current density  $i$  reaches a predefined value. The somewhat arbitrary choice of this cut-off current — values from  $10 \mu\text{A}/\text{cm}^2$  to  $1 \text{mA}/\text{cm}^2$  have been reported — results in differences of the stability data [27].

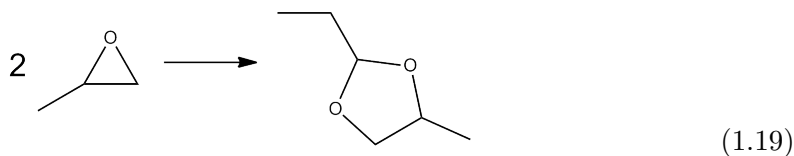
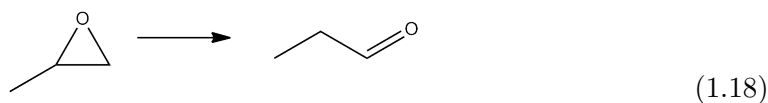
All these variables influence the reported stability values and data from different sources should thus be evaluated with caution.

### 1.3.2 Decomposition under oxidative conditions

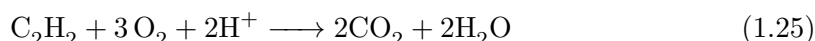
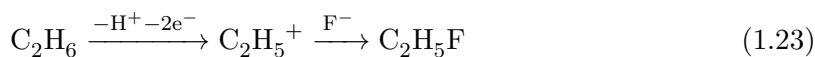
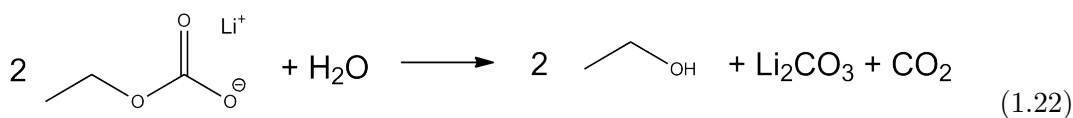
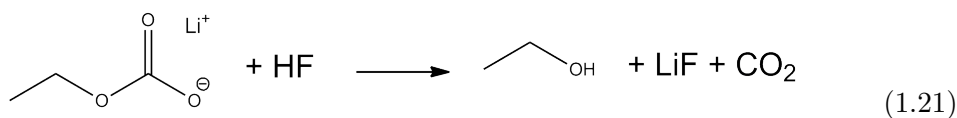
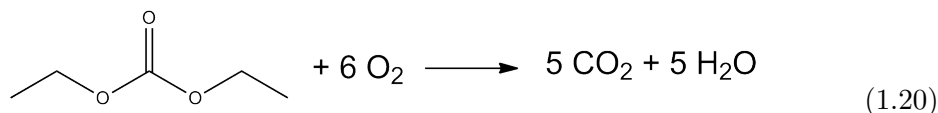
There is significantly less literature available on the oxidation of organic carbonates and the generation of decomposition products than for the reduction process, which may be attributed to the fact that the reduction forms prevalently volatile gases and surface films while the oxidation products are usually soluble in the electrolyte and not easy to detect [24]. All the more the detailed investigation of electrolyte oxidation processes needs to be promoted. The decomposition pathways and mechanisms described in literature which are reproduced below — as reported in literature — are sometimes ambiguous and the data to support these mechanisms hard to find.

Arakawa et al. investigated the oxidative decomposition of PC and EC with  $\text{LiClO}_4$  on graphite via in-situ mass spectrometry and GC/MS in galvanostatic and potentiostatic mode. They proposed the formation of  $\text{CO}_2$ , propanal and 2-ethyl-4-methyl-1,3-dioxolane from propylene carbonate which is initiated and catalysed by an intercalation of the salt anion  $\text{X}^-$  into graphite  $\text{C}_n$  (1.16–1.19). For ethylene carbonate they found the evolution of  $\text{CO}_2$  and other unidentified products at an electrode potential over 5 V [34].





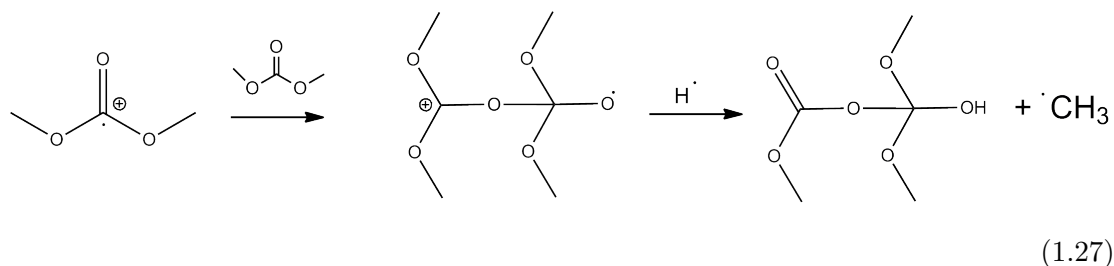
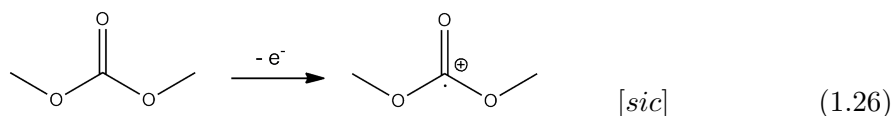
The influence of overcharge for different cathode materials with DEC/LiPF<sub>6</sub> was examined by Kong via GC/MS. Under normal cycling conditions the same compounds, CO, CH<sub>4</sub>, C<sub>2</sub>H<sub>4</sub>, C<sub>2</sub>H<sub>6</sub>, C<sub>2</sub>H<sub>5</sub>F, C<sub>3</sub>H<sub>6</sub> and C<sub>3</sub>H<sub>8</sub>, were found for LiCoO<sub>2</sub>, LiMn<sub>2</sub>O<sub>4</sub> and LiFePO<sub>4</sub>. Unexpectedly, CO<sub>2</sub> was only found with LiMn<sub>2</sub>O<sub>4</sub> and LiFePO<sub>4</sub> but not with LiCoO<sub>2</sub>. Overcharging up to 5 V lead to increased amounts of the observed gases. With LiCoO<sub>2</sub> as electrode material CO<sub>2</sub> was now also observed and C<sub>2</sub>H<sub>2</sub> was generated on LiMn<sub>2</sub>O<sub>4</sub> and LiFePO<sub>4</sub>. The authors mainly hold the O<sub>2</sub> generated from the cathode, analogue reaction (1.55), responsible for the CO<sub>2</sub> evolution (1.20). Also the reaction of Li alkylcarbonates with HF (1.21) and H<sub>2</sub>O (1.22) is assumed to generate CO<sub>2</sub> besides ethanol, although it is unclear whether ethanol actually was detected. A formation mechanism for C<sub>2</sub>H<sub>5</sub>F from ethane was proposed (1.23). The absence of C<sub>2</sub>H<sub>2</sub>, generated by oxidation of C<sub>2</sub>H<sub>4</sub> (1.24), is explained by enhanced O<sub>2</sub> evolution from LiCoO<sub>2</sub> which reacts with C<sub>2</sub>H<sub>2</sub> according to equation (1.25) [35].





Similar experiments were performed by Kumai et al. for  $\text{LiPF}_6$  in PC/EMC/DEC/DMC in a  $\text{LiCoO}_2$ -graphite cell. In the normal charging range mainly  $\text{CH}_4$ ,  $\text{C}_2\text{H}_6$  and  $\text{C}_3\text{H}_8$  were detected. Cells which were overcharged contained mainly  $\text{CO}_2$  and  $\text{CH}_4$  while in overdischarged cells also CO was found. In general the gas volume generated was approximately four times higher in the overdischarged case. Their explanation of the gas generation is in accordance with Gachot [36] for the overdischarged cells and Kong [35] for the overcharged cells [13].

Moshkovich et al. investigated the oxidation of DMC, DMC/EC and DEC/EC with several salts on Au, Pt and Al electrodes by in-situ FTIR, NMR and GC/MS of the solutions. They proposed possible oxidative reaction pathways for DMC and EC. After the initial oxidation of DMC (1.26) the intermediate can react with another molecule of DMC (1.27) or a DMC radical (1.28). The formation of more volatile compounds like CO, formaldehyde and  $\text{CO}_2$  is proposed by reactions (1.29, 1.30). The initiation step for EC is analogous (1.31) but in contrast to reaction (1.29) no volatile aldehyde is formed in (1.32). Also the formation of  $\text{CO}_2$  (1.33), CO, ethanedial and 2-hydroxyacetaldehyde (1.34) are suggested. The reaction with another EC molecule leads to the formation of oligo ether-carbonates (1.35). Although the reactions given in this publication are conceivable, some of them seem to be unlikely. It is noteworthy that Ohsaki and co-workers found evidence that during the overcharge of a  $\text{LiCoO}_2$ -carbon LIB with an EC/EMC/ $\text{LiPF}_6$  electrolyte CO and  $\text{CO}_2$  were generated at the cathode while  $\text{H}_2$ ,  $\text{CH}_4$ ,  $\text{C}_2\text{H}_4$ ,  $\text{C}_2\text{H}_6$ , CO and  $\text{CO}_2$  were formed at the anode side [37]. This is an indication that not only the cathode is involved in the gas evolution during overcharge.

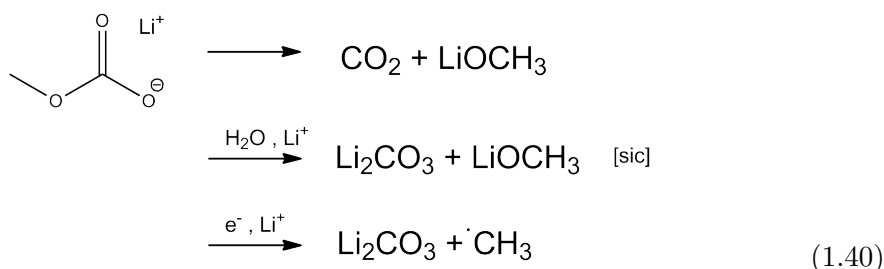
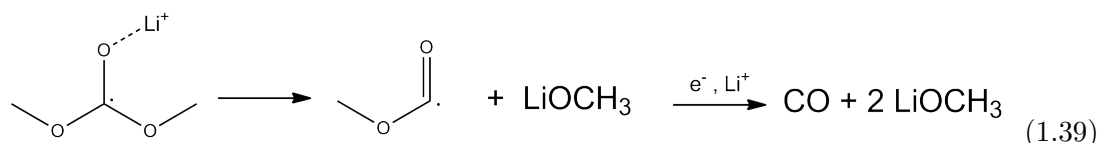
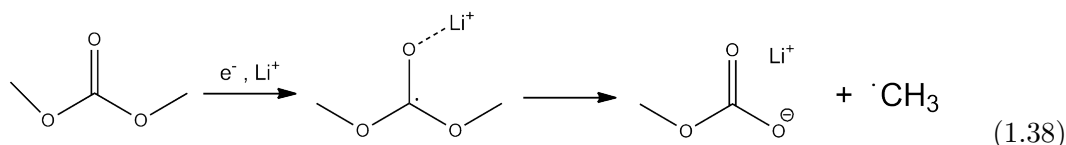
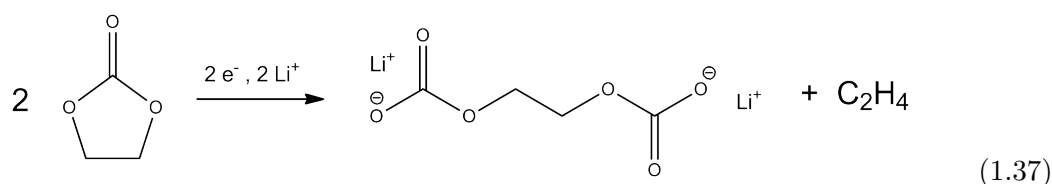
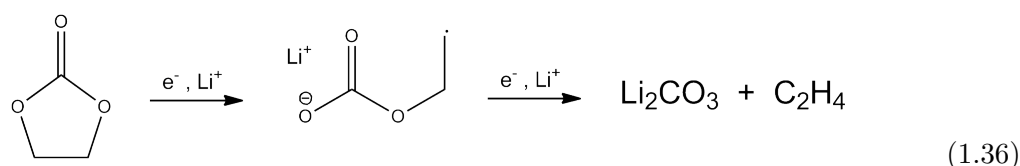




### 1.3.3 Decomposition under reductive conditions

The mechanism for the complex reductive decomposition pathways is generally believed to be initiated by an electron transfer to an organic carbonate like EC (1.36, 1.37) or DMC (1.38, 1.39). The exact details of the reaction cascade of this initiation are still under debate. Especially the discrimination between electrochemically and thermally induced reactions is difficult.

The reduction of EC leads to the formation of solid precipitations of Li carbonates and alkyl carbonates on the electrode surface and gaseous compounds like ethylene. It is also the source for a series of soluble and insoluble oligomeric compounds based on the  $[-CH_2-CH_2-O-]$  unit.



It was suggested that Li methanolate (MeOLi), which is the main product from DMC reduction besides  $\text{CO}_2$  and CO (1.38, 1.39, 1.40), induces a whole series of secondary

reactions which cause a broad spectrum of products [38]. Once formed it readily reacts with EC to produce a series of oligomeric alkyl carbonates (1.41). The successive reactions of the derived products lead to a variety of compounds which are categorised according to Figure 1.4 [39]. Dimethyl-2,5-dioxahexane carboxylate (DMDOHC) was the first of these reported. Examining the effect of MeOLi addition Tarascon and co-workers found an increased amount of dimethyl ether and  $\text{CO}_2$ , presumably formed by reaction (1.42). They also propose a mechanism for the formation of alkyl fluorides and  $\text{POF}_3$  from the reaction of an Li alkoxide with  $\text{PF}_5$  (1.43). Due to traces of  $\text{H}_2\text{O}$  in the electrolyte the formation of methanol is often observed (1.44). The radicals formed in the electrochemical initiation step (1.38, 1.39) are believed to form methyl acetate (1.44), methyl formate (1.46), methane (1.47) and ethane (1.48) [36].

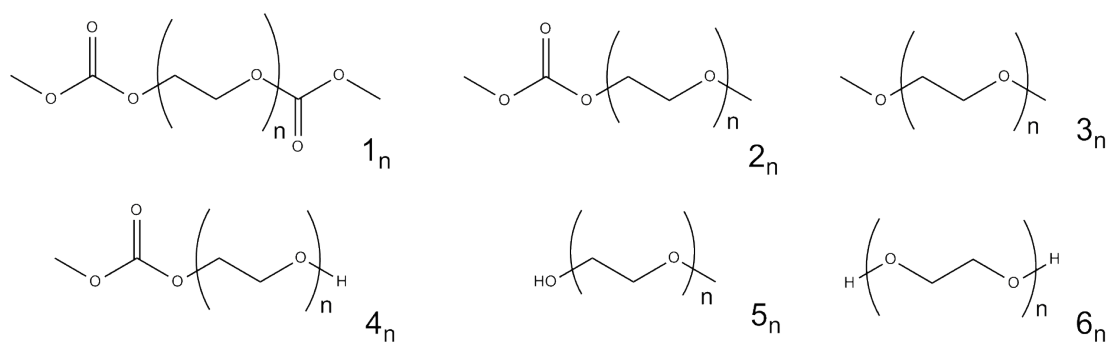
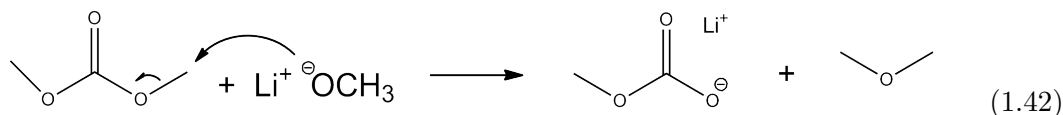
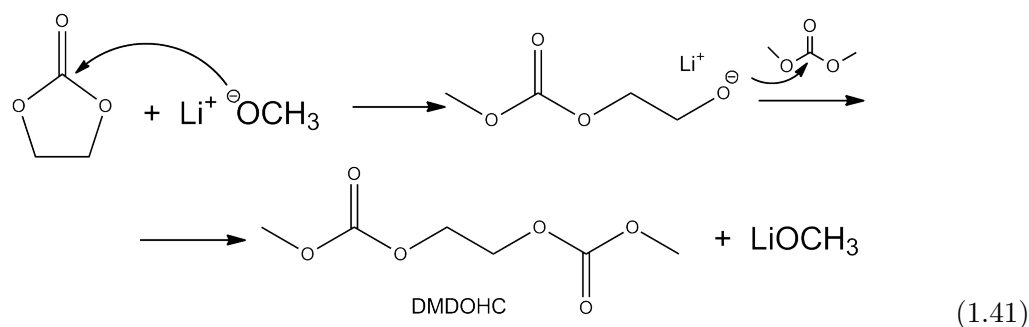
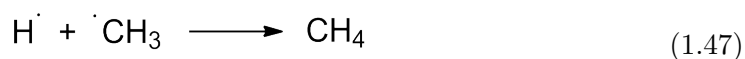
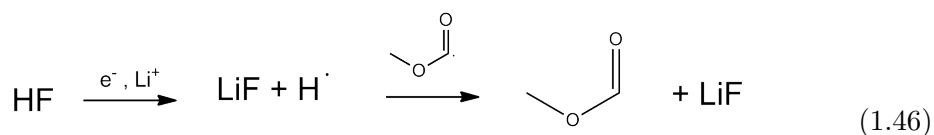
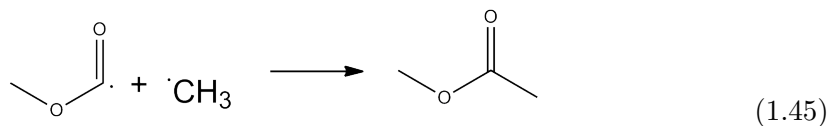
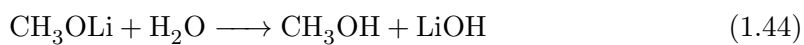


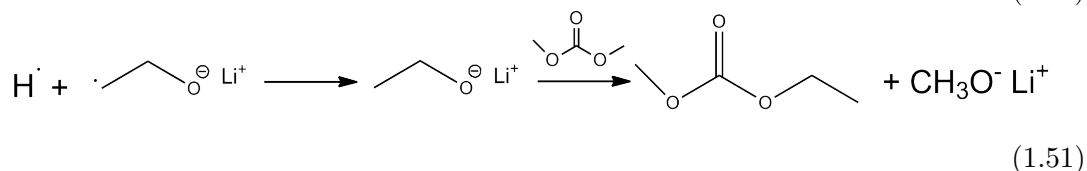
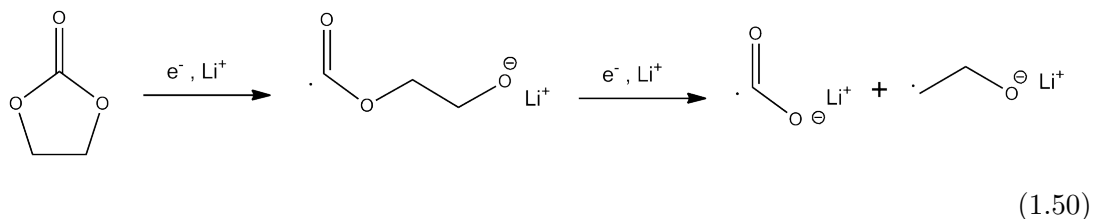
FIGURE 1.4: Series of oligomeric decomposition products reported in literature.





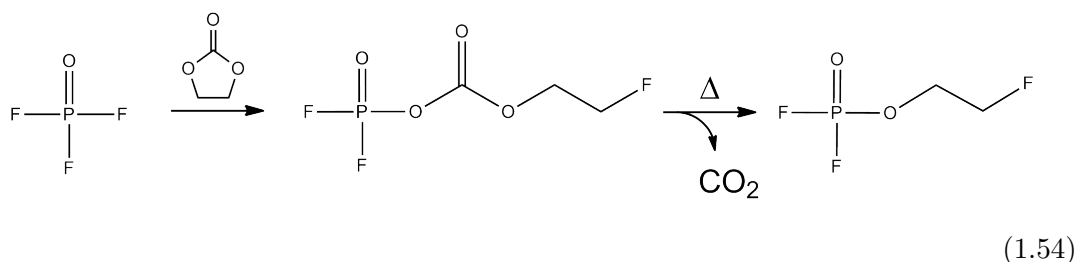
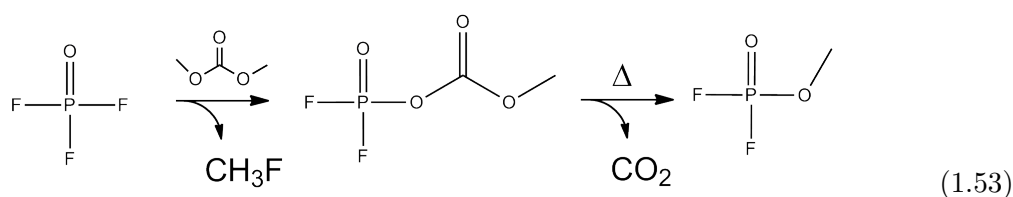
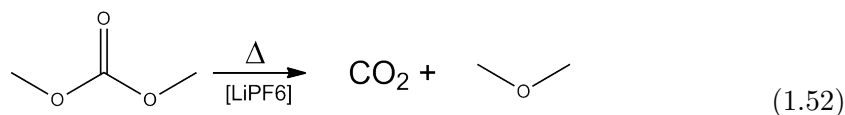
Most of the literature deals with the decomposition of DMC and EC but it is likely that other carbonates react similarly. It is a general trend that the decomposition products from linear carbonates are often volatile while cyclic carbonates lead to low volatile and insoluble compounds.

There have been reports that mixtures of carbonates change their composition during cycling. A transesterification reaction was proposed by Yamachi et al. (1.49) [40] whereas Ogumi and co-workers assume the participation of Li alkoxide species [38] and also the formation of EMC from EC and DMC was reported (1.50, 1.51) [13, 36].

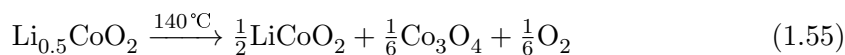


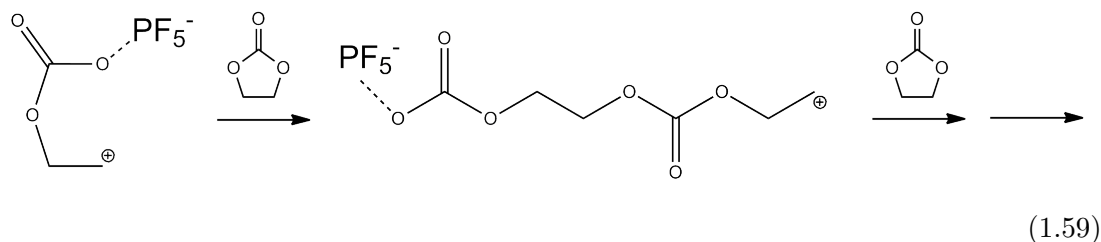
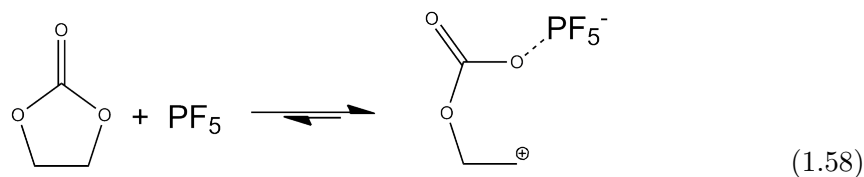
### 1.3.4 Thermally induced reactions

Laruelle and co-workers investigated the thermally induced electrolyte degradation and the influence of  $\text{LiPF}_6$ -addition by GC/MS. An enhancement of the DMC decomposition to  $\text{CO}_2$  and dimethyl ether (1.52) by addition of  $\text{LiPF}_6$  was observed. This corroborates the hypothesis that  $\text{PF}_5$  reacts with water traces under the formation of  $\text{HF}$  and  $\text{POF}_3$  (1.15) which then attacks the solvent molecules (1.53,1.54). In contrast to DMC the reaction of EC produces no volatile alkyl fluorides [36, 39].

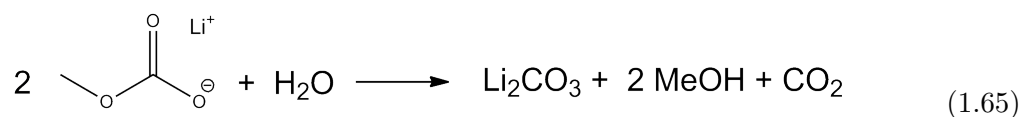
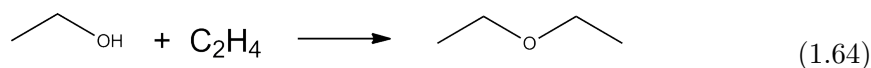
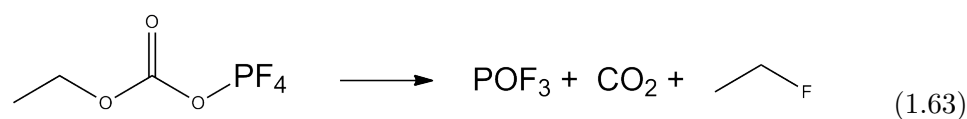
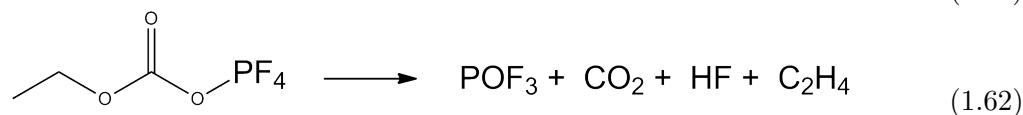
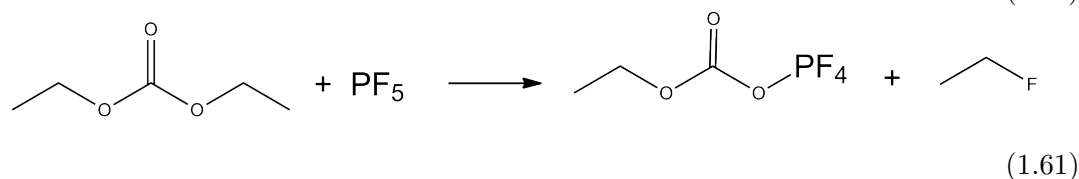
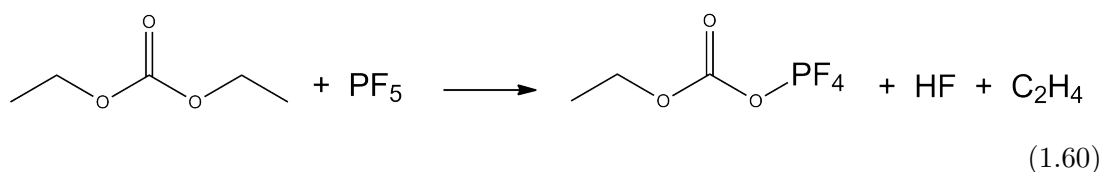


The decomposition and oxygen release (1.55, 1.56) from overcharged  $\text{Li}_{0.5}\text{CoO}_2$  was found to happen around  $140^\circ\text{C}$  and may be enhanced if solvents are present [41]. The generated oxygen then readily reacts with the present solvents (1.57) to form  $\text{CO}_2$  and  $\text{H}_2\text{O}$ . Roth and co-workers also propose a  $\text{PF}_5$ -activated ring-opening (1.58) of EC which then either decomposes to  $\text{CO}_2$ ,  $\text{C}_2\text{H}_4$ ,  $\text{C}_2\text{H}_5\text{F}$  or reacts with solvent molecules to form a series of linear oligo ether-carbonates (1.59).





The thermally initiated reactions of DEC with  $\text{LiPF}_6$  over  $140^\circ\text{C}$  have been investigated by differential scanning calorimetry [42]. A reaction cascade initiated by the Lewis acid  $\text{PF}_5$  was suggested (1.60,1.61). The intermediate then decomposes into  $\text{POF}_3$ ,  $\text{CO}_2$ ,  $\text{C}_2\text{H}_4$ ,  $\text{HF}$  and  $\text{C}_2\text{H}_5\text{F}$  (1.62,1.63). However the authors of this study did not find any evidence for the analogous reaction (1.60,1.61) of DMC. They also concluded that traces of water are involved in the generation of alcohols from lithium carbonate species in the SEI (1.65) and subsequent ether formation (1.64).



In a recent publication Gachot et al. have analysed the gaseous decomposition products via gas chromatography where a parallel FTIR and MS detector was used to disambiguate the identification. From a charged anode heated with an ED/DMC/LiPF<sub>6</sub> electrolyte they identified CO, CO<sub>2</sub>, C<sub>1</sub>–C<sub>2</sub> hydrocarbons and fluorine compounds, linear ethers, formaldehyde as well as methyl formate, methyl acetate and their derivatives. The gases of a swollen LIB were found to contain CO, CO<sub>2</sub>, saturated C<sub>1</sub>–C<sub>4</sub> hydrocarbons and furthermore their fluorinated analogues [43].

### 1.3.5 Techniques for the analysis of evolved gases from lithium ion batteries

As elaborated by Gachot and co-workers [36] the elucidation of electrolyte decomposition mechanisms is a challenging task which cannot be done by gas analysis alone. Many studies have dealt with the soluble products and solid precipitations formed in LIBs. The combination of many techniques can form a better understanding of the decomposition processes going on in a cell. The analysis of evolved gases is, however, of particular importance in this context. On one hand side the evolution of highly flammable and potentially toxic gases in LIBs is a big safety issue and in contrast to soluble products gases are volatile and cause a pressure increase in the cell. On the other hand gas analysis is a handy way to monitor reactions in batteries of most types in-situ and without disturbing the cell chemistry too much.

The techniques established to analyse the gases evolved in LIBs can be divided in two categories. *Ex-situ* or *post-mortem* analysis is the most used approach. Mostly cylindrical cells, like the 18650-type, or pouch cells are prepared and undergo a certain charging program or temperature treatment. Afterwards the cell is opened or pierced with a device that allows the quantitative collection of the generated gases which are injected in the analysis instrument (GC/MS or GC/MS/FTIR [43]) afterwards. This approach has the advantage of easy accessibility and the analysis of large gas volumes giving high sensitivity. The obvious drawback is the lack of temporal resolution to monitor the reactions during the charging or temperature program.

The second approach is far less used as it requires a high level of technical finesse. *In-situ* measurements are usually done by *differential electrochemical mass spectrometry* (DEMS). The classic DEMS-cell is an electrochemical cell where the working electrode consists of a porous membrane (usually PTFE) which is hydrophobic towards the



hydrophilic electrolyte. On one side the membrane can be coated with the working electrode material and on the other side it is connected to the vacuum of the mass spectrometer. Products formed in the electrolyte will evaporate through the membrane and can be detected in the mass spectrometer. It shows a high temporal resolution but the lack of analyte separation causes a complex overlap of mass spectra and complicates the interpretation. The cells are often operated with a constant electrolyte exchange flow [44].

A recently published technique has improved this approach with the construction of a *headspace*-cell [45, 46]. This cell consists of two flat plates which are positioned with a narrow gap in between. The electrode materials are coated on these plates and a steady electrolyte flow between them is established. The gas space or *head space* above the electrolyte level is purged by an inert gas and the evolved gases are transferred into the mass spectrometer through a capillary. This cell allows for more flexibility of the experimental design in terms of electrode material and temperature control.

In this work a new approach was developed for in-situ gas measurement. Through combination of a headspace cell and an FTIR-spectrometer coupled to a GC/MS we could measure the gas evolution in LIBs in conditions which are as close as possible to real world cells. The physical separation of the cell and the instrument allows more freedom in choosing the type of headspace cell and provides additional safety for the instrument in the case of unexpected reactions.

## 1.4 Gas Chromatography / Mass Spectrometry

Gas chromatography/mass spectrometry (GC/MS) is a powerful tool for the analysis of complex mixtures. Gaseous or vaporised compounds are injected into the analytical column where they are separated according to their polarity and volatility. The columns usually consist of fused silica capillaries that are internally coated with a thin film of a stationary phase. Leaving the chromatography column the analytes enter the mass spectrometer where they are ionised by e.g. an electron source. The ionisation leads also to fragmentation of the compounds and the obtained molecular and fragment ions are detected according to their mass to charge ratio. Comparison of the recorded mass spectra with library spectra allows the identification of the compounds. Further details about this technique can be found in suitable textbooks, e.g. ref. [47].

## 1.5 Fourier Transform Infrared Spectroscopy

Fourier transform infrared spectroscopy (FTIR) has found wide spread use in the characterisation of LIBs. With different measurement geometries it was used to investigate analytes in solution and on electrode surfaces. With appropriate instrumentation also the gas phase is accessible. The identification of analytes based on their characteristic absorption bands is highly successful and extensive libraries are available. The fundamental vibrations of organic molecules are typically found in the mid-infrared range — 4000-400  $\text{cm}^{-1}$ . The applicability of the method can be limited by the high complexity of mixtures and also the sensitivity is rather low compared to GC/MS. With the development of FTIR, infrared spectroscopy has become a very fast method — one scan typically takes around 300 ms, while several ten to hundred scans are co-added to yield one spectrum — with high spectral resolution. More information about FTIR can be found in corresponding textbooks like in ref. [48].

## Chapter 2

# Experimental Part

### 2.1 Materials

#### 2.1.1 Consumables

The following solvents and salts were obtained from the *SelectiLyte* product line of *Merck (Darmstadt, Germany)*: Dimethyl carbonate ( $\geq 99\%$ ,  $\text{H}_2\text{O} \leq 20$  ppm, methanol  $\leq 30$  ppm), ethylene carbonate ( $\geq 99\%$ ,  $\text{H}_2\text{O} \leq 20$  ppm, ethylene glycol  $\leq 30$  ppm), *LP30* (DMC/EC 1:1 by weight, 1 M  $\text{LiPF}_6$ ,  $\text{H}_2\text{O} \leq 20$  ppm,  $\text{HF} \leq 50$  ppm). Lithium ribbons (99.9 % trace metal basis, 0.38 mm thickness) and  $\text{LiPF}_6$  salt (battery grade,  $\geq 99.99\%$  trace metal basis) were purchased from *Sigma-Aldrich (St. Louis, MO, USA)*. Stainless steel coin cell parts (cases, spacers, wave springs) for 2032-type cells were obtained from *MTI corporation (Richmond, CA, USA)*, where the cathode side lids were Al-coated. The precoated  $\text{LiCoO}_2$ -electrodes on Al-current collectors were delivered by *Pi-Kem (Staffordshire, UK)* (total thickness: 0.1 mm, current collector: 15  $\mu\text{m}$ , 95.7 % active material). Woven polyethylene fiber separators (thickness: 0.1 mm) had been provided by the company *Freudenberg Vliesstoffe (Weinheim, Germany)* and circular parts of diameter 18 mm were cut. Glass fiber separators (diameter: 18 mm, thickness: 1 mm) have been used from stock at the Austrian Institute of Technology.

Glass head space crimp vials and aluminium seals with silicone septa were obtained from *Restek (Bellefonte, PA, USA)*. All handling of air or moisture sensitive materials and cell assembly was conducted in a Ar-filled glove box by *MBRAUN (Garching, Germany)* ( $\text{O}_2 \leq 0.1$  ppm,  $\text{H}_2\text{O} \leq 0.1$  ppm). The gas sampling cell model *ECC-DEMS* was purchased

from the company *EL-CELL (Hamburg, Germany)*. The *Swing 4400* batteries from *Boston Power (Westborough, MA, USA)* were used for the tests with commercial cells. All experimental work has been performed at the Austrian Institute of Technology, Mobility Department - EDT, located at Giefinggasse 2, 1210 Vienna, Austria. The powder X-ray diffraction and X-ray fluorescence measurements have been conducted by Raad Hamid from the Austrian Institute of Technology.

### 2.1.2 Electrodes

The glassy carbon electrodes, also known as vitreous carbon, were obtained from the company *Mersen (Courbevoie, France)* (grade V25, open porosity 0 %, sulphur  $\leq 50$  ppm). They are widely used as inert working electrodes therefore they were chosen to distinguish the influence of the cathode material on the electrolyte decomposition process. The glassy carbon (GC) discs had a diameter of 15.2 mm and a thickness of 1.80–2.15 mm. Before their use they were polished with sandpaper of grits 320, 600, 2500 and 4000 successively. Afterwards they were cleaned in an ultrasonic bath with water and acetone and then dried.

Precoated cathodes with  $\text{LiCoO}_2$  on Al-foil from *Pi-Kem* were used as a real cathode material. They were calendered from 0.1 to 0.08 mm, cut to circular electrodes of diameter 15 mm, weighted and vacuum dried overnight at 120 °C. Circular counter electrodes with 15 mm diameter were also cut from the lithium ribbons inside the glove box. For the preliminary experiments electrodes were isolated from the *Swing 4400* cell. After discharging the battery it was carefully cut open and the electrodes were removed. The coating was removed from one side of the current collector and again circular electrodes were cut and dried.

### 2.1.3 Boston Power – Swing 4400

The *Swing 4400* cell from *Boston Power*, subsequently also called *Boston Power Cell (BPC)*, has a nominal capacity of 4400 mAh at a nominal voltage of 3.7 V [49]. The specified operating temperature range is -10 to 60 °C for charging and -40 to 70 °C for discharge with a recommended charging current of 0.7 C up to 4.2 V.

It has a graphitic carbon anode and the cathode active material is a mixture of  $\text{LiCoO}_2$  and  $\text{LiMn}_2\text{O}_4$  with an approximate fraction of 78 wt % and 22 wt %, respectively, as was

determined by powder X-ray diffraction and X-ray fluorescence analysis. The electrolyte composition was determined by GC/MS analysis of a small amount extracted from an opened cell which was diluted 1:200 in  $\text{CH}_2\text{Cl}_2$  on the Rtx-5MS column. A dilution series of the main components in  $\text{CH}_2\text{Cl}_2$  was prepared and the quantitative composition of the electrolyte was determined via a linear calibration over the peak areas.

## 2.2 Instruments

### 2.2.1 Electrochemical Equipment

Electrochemical measurements, i.e. cyclic voltammetry and battery charging programs, were performed on a *BioLogic VSP*-potentiostat with a *VMP3B-20* booster channel. All potentials given in this work are defined versus the  $\text{Li}/\text{Li}^+$  redox couple, unless stated otherwise. Following the IUPAC convention cathodic currents are defined with a negative sign and anodic currents with a positive sign. The onset potential of the reactions in the cyclic voltammogram was evaluated by the tangent method. This was chosen as the current signals in the different experiments varied strongly and an estimation via the current density seemed unreliable.

The constant current cycling of coin cells during the preliminary experiments was performed on an *8 Channel Battery Analyser BST8* from *MTI corporation*.

### 2.2.2 GC/MS

A gas chromatograph/mass spectrometer of the model *GCMS-QP2010 Plus* was provided by the company *Shimadzu (Duisburg, Germany)* in the frame of the *SiLithium* project. Helium 6.0 was used as a carrier gas and the injection port was equipped with a heatable automatic 10-port switching valve operated as a 6-port valve (Figure 2.1) with a sample loop of volume 500  $\mu\text{L}$ . The split/splitless injection port was used with a splitless deactivated fused silica liner. Initially the gas chromatograph was equipped with a Rtx-5MS fused silica capillary column from *Restek* (Table 2.1). This rather apolar column has a poly-dimethyl-siloxane (5 % diphenyl-siloxane) stationary phase and allows the separation of a wide spectrum of substances.

In the last part of the project the focus was shifted to the permanent gases evolving

from the cells. As the Rtx-5MS column was not able to separate gases like  $\text{CO}_2$ ,  $\text{O}_2$ ,  $\text{CH}_4$ ,  $\text{C}_2\text{H}_6$  the GC/MS was equipped with a new *Porous layer open tubular*-column (PLOT) *Rt-Q-PLOT MS* (Table 2.1). This setup consisted of a guard column in front of the PLOT-columns and a particle trap installed after the analytical column to protect the mass spectrometer from dislodged particles. The mass spectrometer was equipped with an electron impact ion source (70 V, 150 mA) and a quadrupol mass analyser. In contrast to argon, the use of helium to purge the analytes into the GC/MS enables the detection of fragment ions with an  $m/z$  even below 10. Unfortunately hydrogen ( $m/z = 2$ ) is not accessible to measurement using the scanning mode of the instrument without measuring also helium. It was therefore not determined in the conducted experiments. To detect it a mass spectrometer program based on selected ion channels could be used. The parameters of the used GC/MS methods are listed in Table 2.2 — Table 2.4.

The data evaluation was done with the program *GCMS Solution* using the *NIST Mass Spectral Library, version 11* and the *Wiley Registry of Mass Spectral Data, 9<sup>th</sup> edition*. For identification purposes the mass spectra were averaged over the whole peak and the surrounding background subtracted. Afterwards the identification was done by comparison with the results of the built-in similarity search engine. The quantitative integration of the peaks was done using the signal of a characteristic ion of the analyte, rather than using the total ion current (TIC) since it gives a better selectivity versus background influences. Unless it was interfered by an adjacent peak or the background the ion with the highest intensity was chosen.

For the evaluation of the measurement series of the in-situ experiments a integration

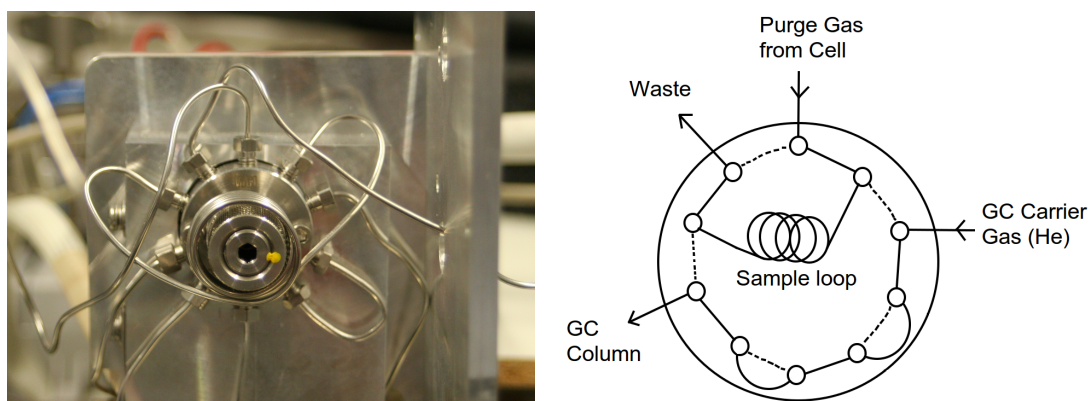


FIGURE 2.1: Left side: Photograph of the 10-port sampling valve. Right side: Scheme of the port connections. The internal switching connections between the ports are shown for the sample loading position (solid lines) and injection position (dotted lines).

method was created in the *GCMS Solution* software which allowed the batch processing of the large amount of data files. After exporting the chromatogram data to ASCII files selected data were transferred into a single text file by a short, self-written FORTRAN program. The peak areas extracted this way were then used to characterise the gas evolution during the experiment and for developing the multivariate model for FTIR.

TABLE 2.1: Specifications of chromatography columns used.

Columns	Stationary Phase	Length	Inner Diameter	Film thickness
Rtx-5MS	Dimethylsiloxane (5 % Diphenylsil.)	30 m	0.25 mm	0.25 $\mu$ m
Rt-Q-BOND	Divinylbenzene	30 m	0.32 mm	10 $\mu$ m
Guard column	medium polarity deactivated	5 m	0.32 mm	
Particle Trap	none	2 m	0.32 mm	

TABLE 2.2: GC/MS parameters of method A

Injection Temperature	200 °C
Linear Velocity	40 cm/s
Column Flow	1.23 mL/min
Column Head Pressure	66.0 kPa
Purge Flow	2 mL/min
Split Ratio	6
Analytical Column	Rtx-5MS
Oven Program	40 °C (2 min) – 30 °C/min – 250 °C (3 min)
Ion Source Temperature	200 °C
Interface Temperature	200 °C
Detector Voltage	1.15 kV
Scan range	10–400 m/z

TABLE 2.3: GC/MS parameters of method B

Injection Temperature	150 °C
Linear Velocity	40 cm/s
Column Flow	1.23 mL/min
Column Head Pressure	66.0 kPa
Purge Flow	6 mL/min
Split Ratio	5
Analytical Column	Rtx-5MS
Oven Program	40 °C (3 min) – 30 °C/min – 200 °C (4 min)
Ion Source Temperature	200 °C
Interface Temperature	200 °C
Detector Voltage	1.2 kV
Scan range	10–300 m/z

TABLE 2.4: GC/MS parameters of method C

Injection Temperature	100 °C
Linear Velocity	50 cm/s
Column Flow	2.38 mL/min
Column Head Pressure	75.3 kPa
Purge Flow	1 mL/min
Split Ratio	8
Analytical Column	Rt-Q-BOND
Oven Program	35 °C (2.25 min) – 20 °C/min – 190 °C (7 min)
Ion Source Temperature	150 °C
Interface Temperature	130 °C
Detector Voltage	1.3 kV
Scan range	10–300 m/z

### 2.2.3 FTIR Spectrometer

The spectrometer and wave-guide system was constructed and provided by Wolfgang Märzinger from the company *i-red* in the frame of the *SiLithium* project. It consists of a electronic control device and an integrated interferometer unit with a globar as light source. The interferometer optical system is purged with nitrogen gas and connected to a hollow wave-guide made of a silver halide coated fused silica capillary (length: 1 m, ID: 0.5 mm) . The light enters the wave-guide trough a  $\text{MgF}_2$ -window at one end and reaches the peltier-cooled CCD-detector after passing the inner gas volume and the outlet window. The hollow wave-guide has gas entry ports at both ends which allows sample or purge gas to flow through the inner waveguide volume. This way the optical path length of the infrared beam and the sensitivity are maximised even for small gas volumes. The available spectral range goes from  $\sim 1500\text{--}3600\text{ cm}^{-1}$ . The hollow wave-guide was embedded in a thermally insulating sleeve together with a heating wire to avoid condensation of products inside the wave-guide and kept at a temperature of 55 °C. Based on the GC/MS data a multivariate model for the concentrations of several analytes was developed by Wolfgang Märzinger which allows to monitor the analyte concentrations via FTIR with a temporal resolution below 30 s. For each spectrum recorded, 70 interferograms were averaged which gives one full spectrum every 24 s.



### 2.2.4 Gas Sampling Cells

Two different gas sampling setups were designed in order to investigate self-assembled coin cells and also a high power commercial cell, namely *Swing 4400* from *Boston Power* (*St.Louis, MO, USA*). The gas sampling cell for the commercial cell consists of a PTFE container (height: 10.4 cm, ID: 6.2 cm) with a screw-on lid (Figure 2.2). The body has two valves for gas in- and outlet to purge the evolved gases from the cell into the instrument. A cell holder, suitable for the *Swing 4400* cell, is attached to the inner side of the lid and leads for the electrical connection are passed through the lid. A type K thermocouple is installed as well to monitor the battery temperature during the experiment. The inner gas volume of the container, without the battery, is approximately 270 mL. For gas measurements the safety vent of the battery is pierced carefully with a hammer and a sharp screwdriver in order to provide an opening for the evolving gases.

The gas sampling setup for coin cells is made of two parts. First the coin cell is assembled, i.e. the counter electrode (or anode) is placed in the cathode cup, then two layers of separators and the working electrode (or cathode) are placed on the stack. After each part a small amount of electrolyte is pipetted into the cell. Now the cell is filled up with electrolyte. Finally a wave washer to ensure sufficient pressure on the components and the anode lid are placed on top. Four holes of diameter 1.1 mm were drilled into the lid to allow the escape of the evolving gases. The cell is then crimped shut with a crimping machine. It should be noted that the anode is placed at the cathode-marked cup and vice versa. This unusual setting was chosen to ensure that both electrodes are



FIGURE 2.2: Photograph of the PTFE gas sampling cell for the BPC. Cell body (left side) and lid with attached cell and thermocouple (right side).

submersed in the electrolyte. The second part is a *ECC-DEMS* cell from the company *EL-CELL*, Germany. This cell has a stainless steel body made of a bottom and a top lid. Both the bottom and the lid have gas connections for purging through gas (Figure 2.3 a). The previously assembled coin cell is placed, with holes upside, on the bottom of the *ECC-DEMS* cell which has circular channels at the base for better gas purging (Figure 2.3 b). The cell is closed with the upper lid where a gold coated spring ensures electrical contact (Figure 2.3 c). A plastic sealing gasket separates upper and lower part to prevent short circuiting the coin cell. All other ports of the *ECC-DEMS* cell are closed to seal it against the atmosphere (Figure 2.3 d). Figure 2.4 depicts the cross section of the coin cell gas sampling cell. The inner volume of the *ECC-DEMS* cell is approximately 9 mL.

All cell assembling steps described above are performed in an argon-filled glove box.

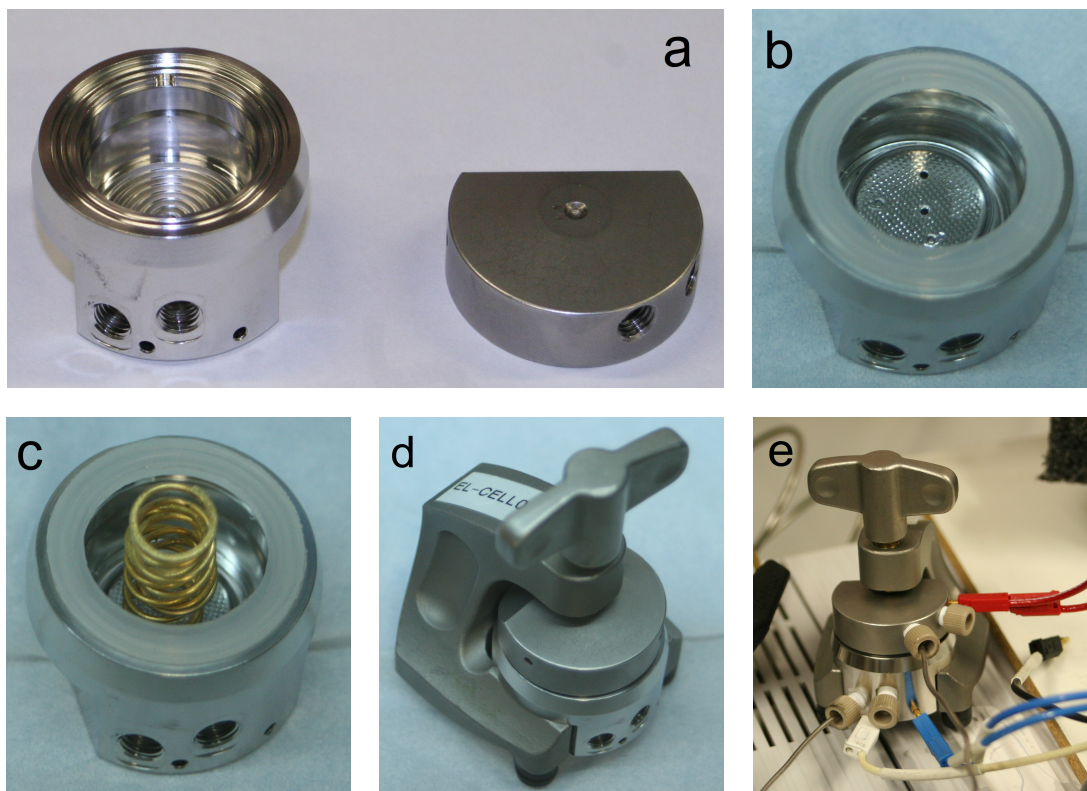


FIGURE 2.3: (a-d): Assembly steps of the coin cell gas sampling setup. (e): Cell with gas and electrical connections (red: working electrode, blue: counter electrode, white: reference electrode).

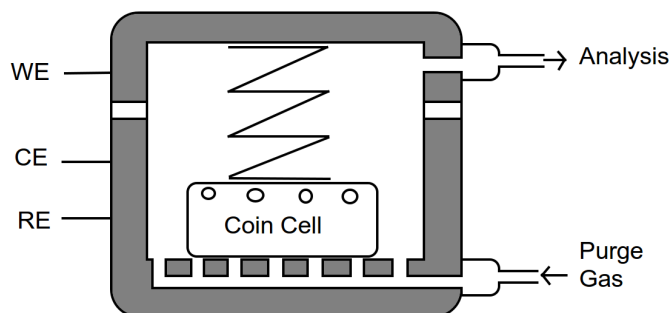


FIGURE 2.4: Schematic cross section of the coin cell gas sampling cell. Electrical connections: Working electrode (WE), counter electrode (CE), reference electrode (RE).

## 2.3 Development of the Gas Measurement Technique

After the startup of the GC/MS instrument first preliminary experiments were performed to explore the potential of the method. The ECC-DEMS cell was cycled and overcharged with electrodes isolated from the BPC or Li metal and various methods to extract the evolved gases from the cells and transfer them to the instrument were tested. Unfortunately no decomposition products could be detected and we assumed that the products could be trapped in the separator due to the unfavourable ratio of separator and evolving gas volumes. Indeed upon placing separators in a sealed headspace vial and heating them it was possible to identify several decomposition products. Using this product spectrum a suitable GC/MS method for analysis was developed.

To go from ex-situ to in-situ measurements a vacuum membrane pump was connected to the waste outlet of the 10-port switching valve and a connection leading to the ECC-DEMS cell to the inlet. This way the gases evolving should be sucked into the sample loop from where they could be injected into the GC/MS. As it was still not possible to collect sufficient amounts of gases directly from the ECC-DEMS cell the focus was shifted to the commercial BPC as larger amounts of gases were expected from the larger cell. It was indeed possible to collect reproducible data from the BPC in the big PTFE gas sampling cell during a step wise overcharging program. To avoid dangerous overheating the temperature of the cell was monitored with a thermocouple attached to the cell body. For better reproducibility the setup was changed from sucking the gases to purging them into the sample loop. The purging gas was later changed from argon to helium as the former was overlapping strongly with the analytes' signal in the mass spectrometer. The purge gas flow was controlled with a needle valve. We decided to focus our investigations on the highly volatile products like permanent gases and light

hydrocarbons as they pose the majority of decomposition products and are more worrisome concerning flammability and toxicity. Therefore the previously installed capillary column was replaced by a PLOT column which is better suited to separate them. Also the method was developed further to a continuous purge flow through the gas sampling cell in contrast to a *stop, charge and purge* flow.

The gas measurement from coin cells was not possible up to this point and we thought of ways to increase the electrolyte amount in the cell. The use of more or thicker separators that could store more liquid was unsuccessful and also the gas inlet at the bottom of the ECC-DEMS cell prevented excessive electrolyte spillage. The idea to modify the ECC-DEMS cell setup from scratch came up and eventually a combination of conventional coin cells with the ECC-DEMS cell was constructed. The relatively large cathode cup is able to hold large amounts of electrolyte which prevents the cell from drying out during the experiment and provides sufficient educt for decomposition reactions. The anode lid was perforated so that the decomposition products could leave the cell and be detected. The whole coin cell was then placed inside the ECC-DEMS cell which was connected to the setup and the gaseous cell contents were purged into the instrument. On connecting the cell to the setup it was crucial to avoid short-circuiting the cell with the metal tubing. With this setup it was possible to measure the gaseous products even with continuous flow as the concentrations are high enough. It is important to mention here that the gas flow has strong influence on the concentration of the measured gases as it dilutes them. The adjustment of the purge gas flow is a balance between too low gas flow, which leads to insufficient purge of the sampling cell and analyte concentrations above the rather narrow dynamic range of the FTIR system, and too high gas flow, resulting in dilution of the analytes beyond the detection limit. Therefore it has to be regulated carefully. The FTIR instrument with the hollow wave guide was then connected to the setup between the gas sampling cell and the GC/MS 10-port switching valve and all gases passed through the hollow wave guide as well as the sampling valve/loop. With the time/concentration profile of a series of experiments obtained from the GC/MS and the simultaneously recorded infrared spectra Wolfgang Märzinger (*i-RED*) developed a multi-variate model based on a partial-least-squares regression for the detected analytes. It was then possible to improve time resolution in the monitoring of evolved gases as the GC/MS was able to produce one data point only every 20 min while the gas FTIR system had a data acquisition interval of below 30 seconds. This is crucial for applying the technique to observe fast processes. The final setup is depicted in Figure 2.5, Figure 2.6



and Figure 2.7. The gas sampling cell is continuously purged with He and the evolving gases pass through the hollow wave-guide and then the GC/MS sample loop. As soon as a GC/MS run is finished the valve switches and injects the content of the sample loop in the GC/MS. During the runs the gases leave the system through the sample valve waste outlet.

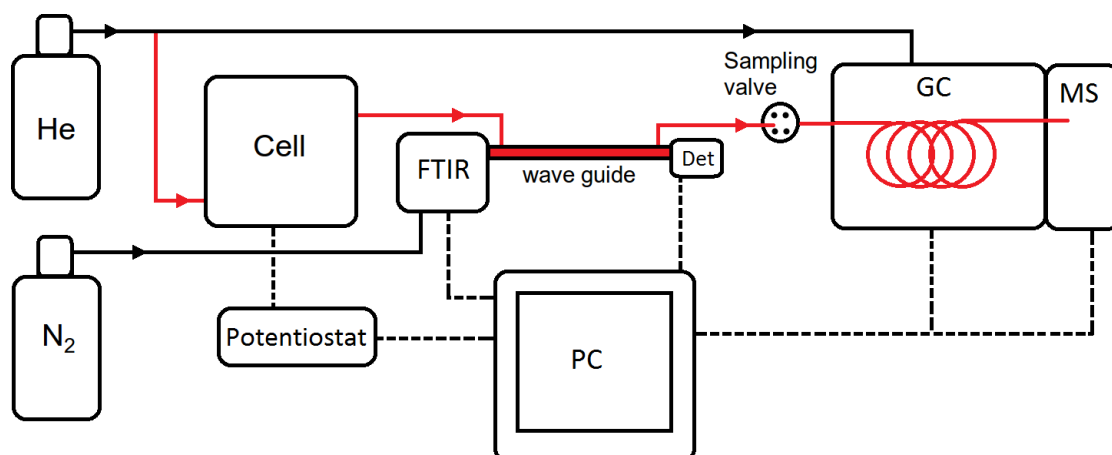


FIGURE 2.5: Scheme of the In-situ gas analysis setup. Solid lines: Gas connections (red = analytic gas path). Dashed lines: Electrical/control connections.



FIGURE 2.6: Photograph of the In-situ gas analysis setup. Visible are the GC/MS instrument (middle) with the FTIR spectrometer on top, the FTIR spectrometer power supply (brown box) with the data storage unit on top and the electrical connections to the potentiostat (black cable) .

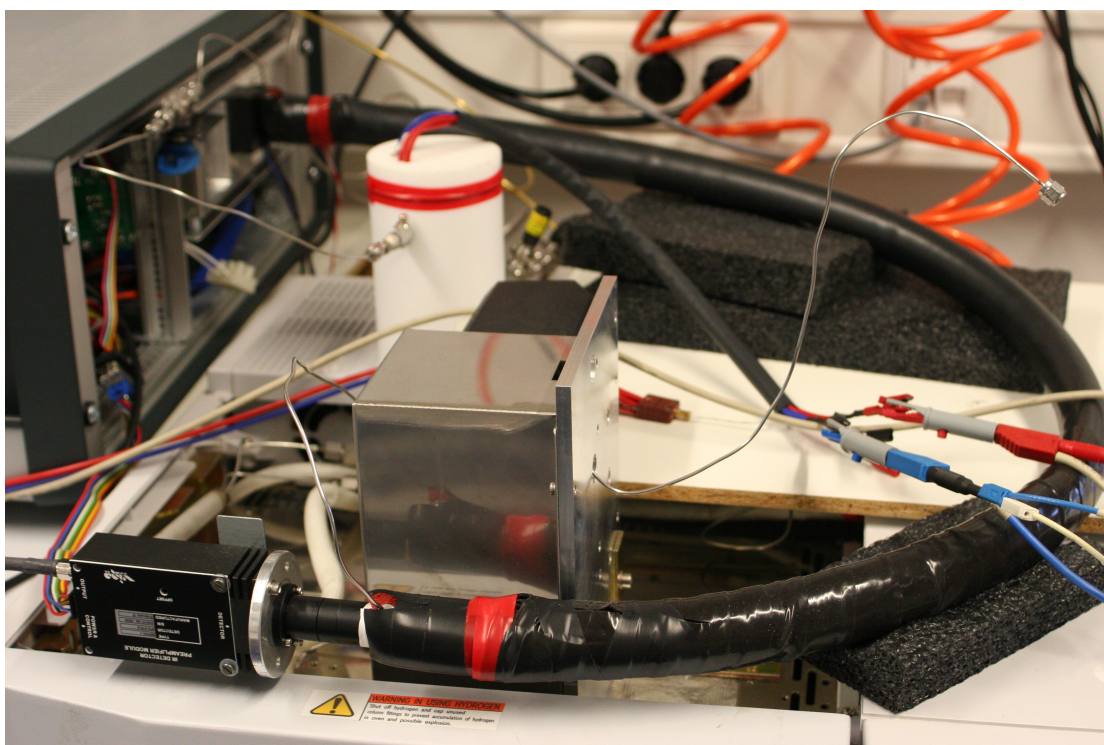


FIGURE 2.7: Photograph of the In-situ gas analysis setup. Visible are the hollow waveguide (black tube) connected to the FTIR spectrometer (rear) and the detector (front, small black box), the PTFE gas sampling cell (white cylinder) with connections and the casing of the 10-port sampling valve (metallic box).

## Chapter 3

# Results and Discussion

### 3.1 Preliminary Experiments

To get a first idea of the product spectrum formed and to optimise the GC/MS method coin cell type cells were assembled with the isolated BPC cathodes. The cells were assembled inside the *ECC-DEMS* cells which allow easy recovery of the separators. The Li anode was placed on the bottom of the cell, a glass fiber separator impregnated with 100  $\mu$ L LP30 and a cathode cut from the BPC cathode on top. The cells were cycled at 25°C between 5 V and 3 V, compare Figure 3.1. It shall be noted that the upper potential limit was chosen above the recommended value of 4.2 V in order to decompose the electrolyte. After cycling the cells were opened in the glove box and the separator transferred quickly into a head space crimp vial which was subsequently closed and placed in an oven at 150°C for 1 h. Afterwards the gas was extracted with a syringe through the septum and injected in the GC/MS for analysis using method A (Table 2.2).

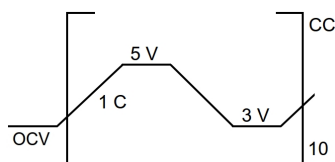


FIGURE 3.1: Cycling program: from open circuit voltage (OCV) between 3 and 5 V at a constant current (CC) charging rate of 1 C for 10 cycles.

The analysis of compounds (cf. appendix A: Figure A.1) released from the heated separators revealed evidence for several decomposition products which are listed in Table 3.1 with their retention time. CAS numbers have been added for unique identification. This method of sample preparation did not allow the analysis of highly volatile substances. Unfortunately not all compounds could be identified unambiguously. Some of them may come from thermally initiated reactions during heating and also reactions involving the materials of the glass fiber separator.

TABLE 3.1: Compounds identified from the separators cycled at 25 °C. Ambiguous identifications are labelled with a question mark. RT: Retention time

Compound (CAS Nr.)	RT (min)
Methyl formate (107-31-3)	1.33
POHF <sub>2</sub> (14939-34-5)	1.38
Methyl acetate (79-20-9)	1.53
1,1-dimethoxy ethane (534-15-6)	1.81
DMC (616-38-6)	1.97
Tetrahydrofuran (109-99-9)	2.02
2-methyl-1,3-dioxolane (497-26-7)	2.19
1,2-dimethoxy ethane (110-71-4)	2.33
EMC (623-53-0)	2.68
1,4-dioxane (132-91-1)	2.75
Ethyl methylphosphonofluoridate (673-97-2)	3.17
Methyl methoxyacetate (6290-49-9)	3.33
Allyl methyl carbonate (35466-83-2) ?	3.52
1-Isopropoxypropan-2-ol (3944-36-3) ?	3.66
1,4-Dimethoxy-butane (13179-96-9)	4.09
2-Methoxyethoxy acetic acid (16024-56-9) ?	4.72
EC (96-49-1)	5.02
1,2,4-Trichloro-heptafluoro-butane (335-45-5) ?	7.24
1,1,3,4-tetrachloro-1,2,2,3,4,4-hexyfluoro-butane (423-38-1) ?	7.29
Butanoic acid anhydride (106-31-0)	8.22
Tris(2-chloroisopropyl)phosphate (13674-84-5)	9.02

### 3.1.1 Swing 4400 Electrolyte Composition

As described in section 2.1.3 the electrolyte of the *Swing 4400* cell was analysed and the composition determined. The main components were identified as dimethyl carbonate, ethylmethyl carbonate, ethylene carbonate and propylene carbonate. Furthermore DEC, biphenyl and other compounds were detected in small amounts (Table 3.2). DEC is thought to origin from EMC (1.49). Biphenyl is a known electrolyte additive acting as an overcharge protection. Also small traces of an ether compound were detected which



is assumed to be the diethylene glycol dimethyl ether (3<sub>2</sub>, Figure 1.4). Several peaks were attributed to decomposition products of the analytical column.

TABLE 3.2: Compounds identified by GC/MS in the electrolyte of the Swing 4400 cell.

Compound (CAS Nr.)	Amount (wt% )
DMC (616-38-6)	$29 \pm 2$
EMC (623-53-0)	$45 \pm 3$
DEC (105-58-8)	traces
EC (96-49-1)	$12.9 \pm 0.6$
PC (108-32-7)	$13.5 \pm 0.7$
Diethylene glycol dimethyl ether (111-96-6)	traces
Biphenyl (92-52-4)	traces

## 3.2 In-situ Gas Measurements

During and after the development of the experimental setup and the analytical procedure it was possible to collect first representative results. Measurements of the gas evolution from coin cells and commercial cells were conducted by the method described in section 2.3. As it was not possible to seal the setup entirely against air, a rather large peak of co-eluting O<sub>2</sub> and N<sub>2</sub> was found in most chromatograms with a retention time of  $\sim 1.40$  min on the PLOT column. It is assumed that this leak is located at the optical window of the hollow wave guide or the 10-port valve. Also water was found due to the same reason with a retention time (RT) around 4.4–4.5 min. For better readability these peaks are not labelled in every figure.

### 3.2.1 Gas evolution from the Swing 4400 cell

#### 3.2.1.1 Cycling in normal voltage range

The first experiment with the *Swing 4400* cell (BPC) was to charge and discharge the cell three times between 4.2 V and 3.0 V with a charging rate of 1 C, corresponding to a current of 4.4 A. In these early experiments the gas sampling cell was not under permanent gas flow-through to concentrate the evolved gases. Instead the cell container was closed, the charging step e.g. up to 4.2 V performed and then the cell content purged into the GC/MS (Method B, Table 2.3). The container was then flushed through to remove all gases and then closed again for the next charging step, e.g. discharge

to 3.0 V. Besides the electrolyte components DMC, EMC and DEC also traces of 2-fluoropropane, acetic acid and methyl acetate were detected during the normal cycling of the cell (Figure A.2). These volatile decomposition products are closely co-eluting with the permanent gases on the Rtx-5MS column and the small peaks were strongly overlapped. Evidence for the identified compounds is shown in the mass spectra of Figure 3.2 and Figure 3.3.

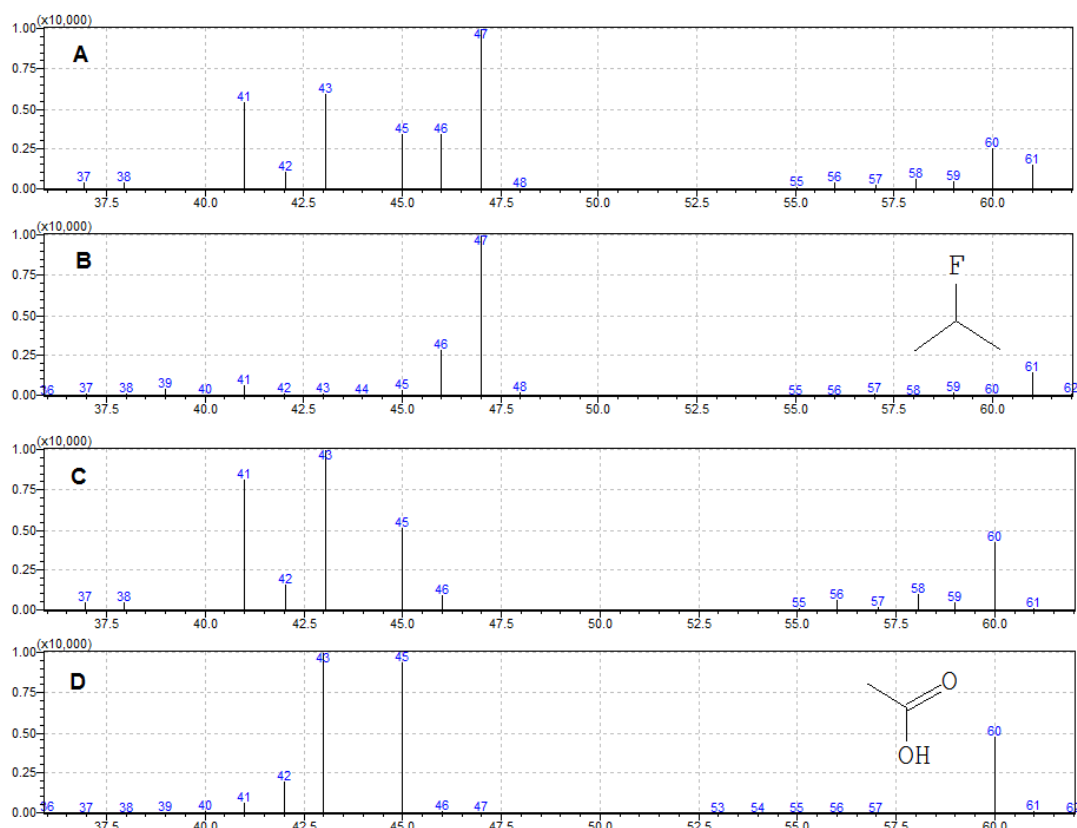


FIGURE 3.2: Mass spectra of 2-fluoropropane and acetic acid detected during normal cycling of the BPC. A: Mass spectrum after background subtraction. B: Library spectrum. C: Subtraction result of A-B. D: Library spectrum.

### 3.2.1.2 Overcharge

After the cycling in the normal voltage range the behaviour of the BPC on overcharging beyond the recommended end-of-charge voltage of 4.2 V was investigated. Therefore the cell was charged to 4.2 V with 1 C and then up to 5 V in steps of 0.2 V. After each charging step a gas measurement by GC/MS was performed as described in section 3.2.1.1. Up to 4.4 V no additional gases other than in the normal voltage range were detected. From 4.6 V on massive evolution of gases started (cf. Figure A.2 and Figure A.3). Together

with the gas evolution also the temperature rose rapidly from  $\sim 30^{\circ}\text{C}$  to  $\sim 50^{\circ}\text{C}$ . The trend of  $\text{CO}_2$  evolution is shown in Figure 3.4 and also the other compounds listed in Table 3.5 follow this trend. Figure 3.5 shows the mass spectra of two unidentified compounds, which may be products of a reactive analyte with the column material. The ions recorded in the permanent gas peak show indications for  $\text{POF}_3$  ( $m/z = 104$  and  $85$ ) and various hydrocarbons. However, their convolution makes an identification hard and a quantification impossible. Therefore the use of a PLOT column was chosen for later experiments which is able to separate most permanent gases and light hydrocarbons. It is interesting to notice that both the gas and heat evolution (data not shown) show two maxima. At  $4.6\text{ V}$  and at  $5.0\text{ V}$  the signal is increasing while it decreases in between.

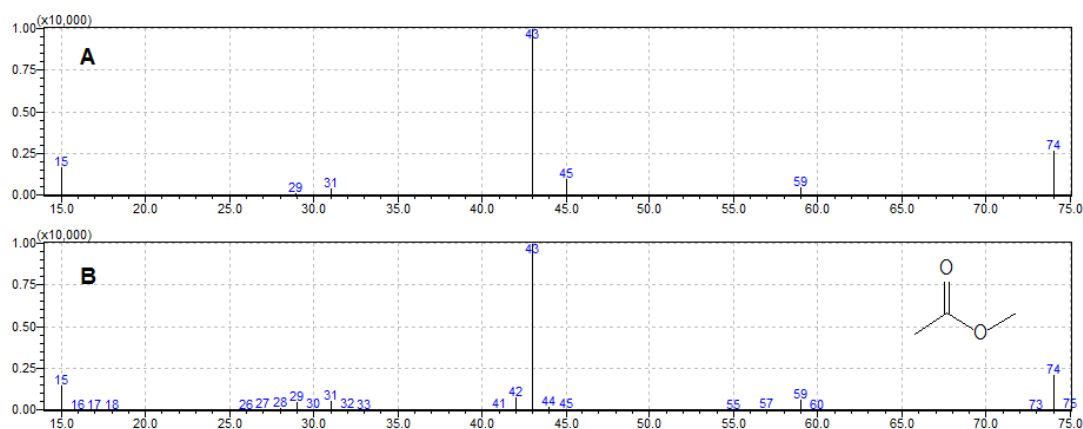


FIGURE 3.3: A: Mass spectrum of methyl acetate detected during normal cycling of the BPC (background subtracted). B: Library spectrum.

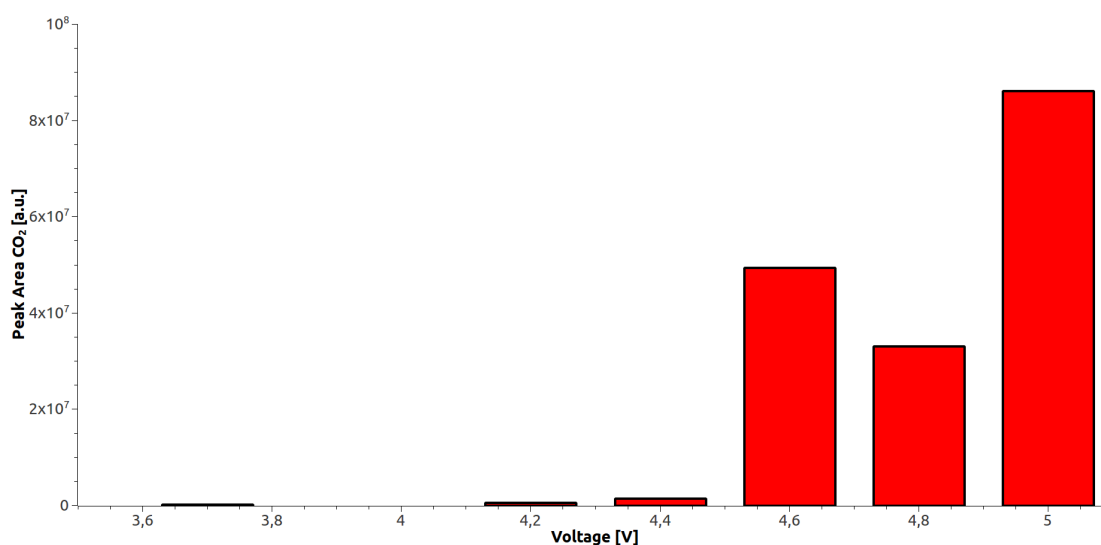


FIGURE 3.4:  $\text{CO}_2$  signal during the overcharge of the BPC.

TABLE 3.3: Compounds identified during the overcharge of the BPC with the Rtx-5MS column. Ambiguous identifications are labeled with a question mark.

Compound (CAS number)	RT / min
CO <sub>2</sub>	1.41
POF <sub>3</sub> ?	1.41
Hydrocarbons ?	1.41
Methyl acetate	1.70
Unidentified	1.73
tert-Butyl(dimethyl)silyl methylphosphonofluoridate?	1.98
2-Hydroxy-2-methyl-propanoic acid ethyl ester (80-55-7)	3.78
3-Methyl heptane (589-81-1)	3.94

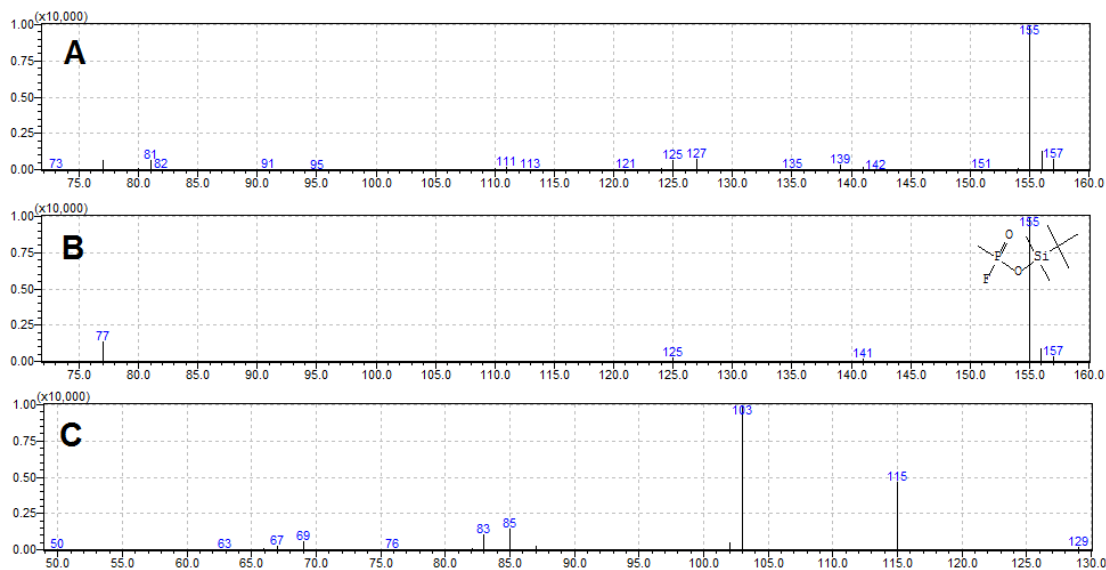


FIGURE 3.5: Mass spectra of unidentified compounds detected during overcharge of the BPC. A: Retention time: 1.98 min. B: Library spectrum of tert-Butyl(dimethyl)silyl methylphosphonofluoridate. C: Retention time: 1.73 min. Compare Figure A.3.

The chromatography column was exchanged for a PLOT column (Method C, Table 2.4) and the overcharge experiment repeated. This time the gas sampling container was not closed between the measurements and there was a continuous flow of purge gas through it. Also the BPC was not charged in steps but continuously. After charging in the normal range, it was charged with a charging rate of 0.7 C (the manufacturer-recommended value) up to 4.2 V, held at constant voltage for 15 min and then charged with 0.2 C up to 5.0 V (Figure A.5). The reduced charging current in the overcharge region was chosen to mitigate the reactions and keep the temperature rise in the cell in a safe range. The charging was stopped when the temperature reached 55°C. During this experiment a large variety of evolving compounds was detected (Figure 3.6). A series of hydrocarbons and also products of secondary reactions was identified (Table 3.4), however, POF<sub>3</sub> was

TABLE 3.4: Compounds identified during the overcharge of the BPC with the PLOT column. Ambiguous identifications are labelled with a question mark.

Compound	Retention Time (min)	Compound	Retention Time (min)
CO	1.41	Methyl bromide ?	7.29
Methane	1.49	Dimethyl difluoro silane	7.50
CO <sub>2</sub>	1.79	Methyl formate	7.54
Methyl fluoride	2.22	Isobutane	7.58
Ethyl formate	9.32	2-methyl-1-propene	7.78
Ethylene	2.43	Butane	7.97
Ethane	2.93	Methoxy ethane	8.14
Fluoro ethane	5.02	Trimethyl fluoro silane	8.90
1,1-Difluoro ethane	5.27	Acetone	8.96
Propene	5.53	Methyl acetate	9.34
Propane	5.74	2-Methyl butane	9.49
Cyclopropane	5.94	Diethyl ether	9.59
Dimethyl ether	6.24	Pentane	9.74
Methanol	6.46	Methyl propionate	11.03
Acetaldehyde	6.82	n-Hexane	11.52
2-Fluoro propane	7.09	Propanoic acid ethyl ester	13.23

not detected in either of the experiments conducted with the PLOT column, so one can assume that it reacts with the column material. Unfortunately also the infrared bands of  $\text{POF}_3$  lie outside the range of our detector making its detection impossible. The trend in the gas evolution and the charging and temperature curves (cf. Figure 3.7) corroborates the observations of the previous experiment that at least two stages appear during the overcharge of the BPC. Figure 3.8 shows the normalised signals for several gas species recorded via GC/MS and also the values obtained from FTIR data (smoothed with a 15-point moving average). The data are plotted normalised since a comparison of the peak areas is not meaningful as the response for each compound is different. However an inspection of the total ion current chromatogram gives an approximate idea of the relative amounts (Figure 3.6).

A first gas evolution was detected by the FTIR around 4.25 V and large increase was found at 4.38 V and 4.57 V. These stages could be related to the decomposition of two different electrolyte components. Unfortunately the data acquisition of the FTIR stopped shortly before the end of the experiment. The comparison of both data sets shows the strengths and weaknesses of the methods. The absolute values from GC/MS are more reliable as they are directly measured. The infrared values on the other hand are based on a model created from the GC/MS data and are therefore inherently prone to higher

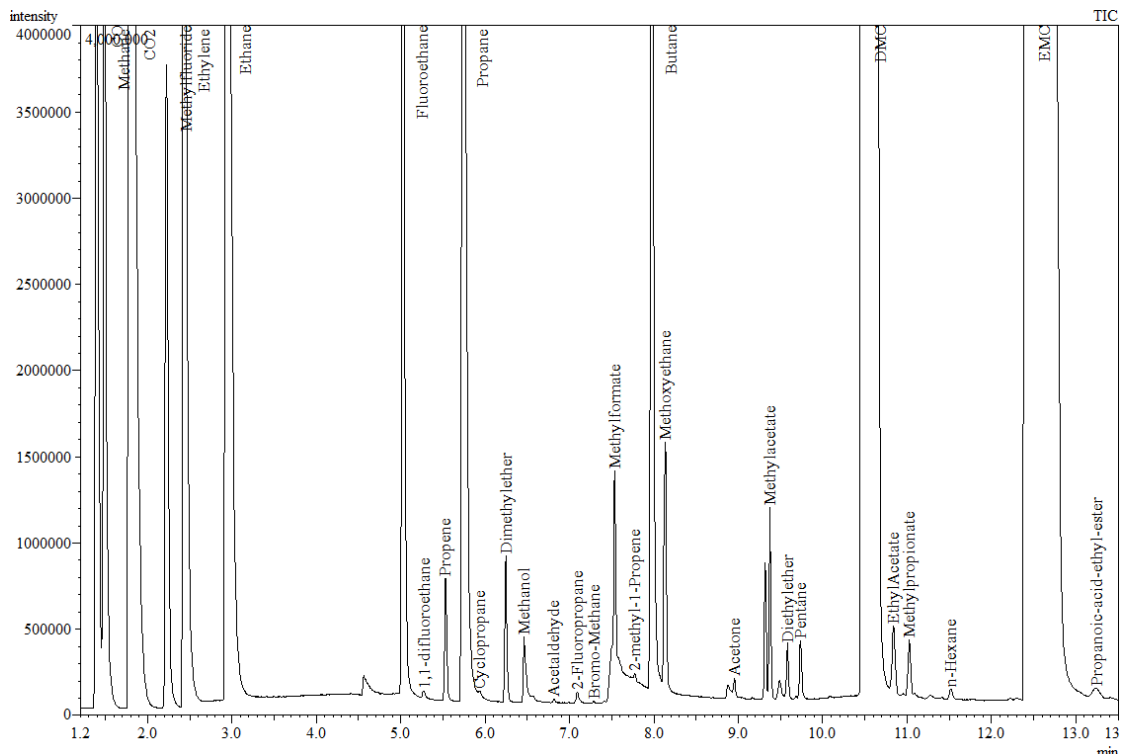


FIGURE 3.6: Gas chromatogram of the compounds evolved from the BPC. Recorded at a charging voltage of 4.75 V .

error and noise. The signal increase in the FTIR data at  $\sim 4.25$  V was not found in the GC/MS data and is thus assumed to be a fluctuation caused by a weakness in the model. In respect of the temporal resolution the FTIR is clearly superior as it shows the gas evolution in much higher time resolution. With the slow recording speed of GC/MS it even seems possible that intermittently formed compounds are not detected. Caution is advisable as some signals show fluctuations that are not in agreement with the GC/MS data. Comparing the values from both methods (Figure 3.8) shows strong fluctuations for  $\text{CH}_4$  in the FTIR which are not detected with GC/MS. The concomitant decrease of  $\text{CH}_4$  and increase of  $\text{C}_2\text{H}_6$  seen around 4.35 V and 4.6 V could indicate a weakness of the model correlating the FTIR to the GC/MS data. The infrared spectra of methane and ethane are very similar and it is very difficult to quantify them in a mixture.

When the experiment was repeated the battery only reached a maximum temperature of  $40^\circ\text{C}$  (Figure 3.7) and also the gas evolution was attenuated so that only the most abundant components were detected. A similar spectrum of species was found and the charging behaviour and heat evolution were comparable. Two possible explanations for the different temperature rise in the second experiment are: It is either different from cell to cell or a slight change in the purge gas flow, which has a cooling effect, kept the

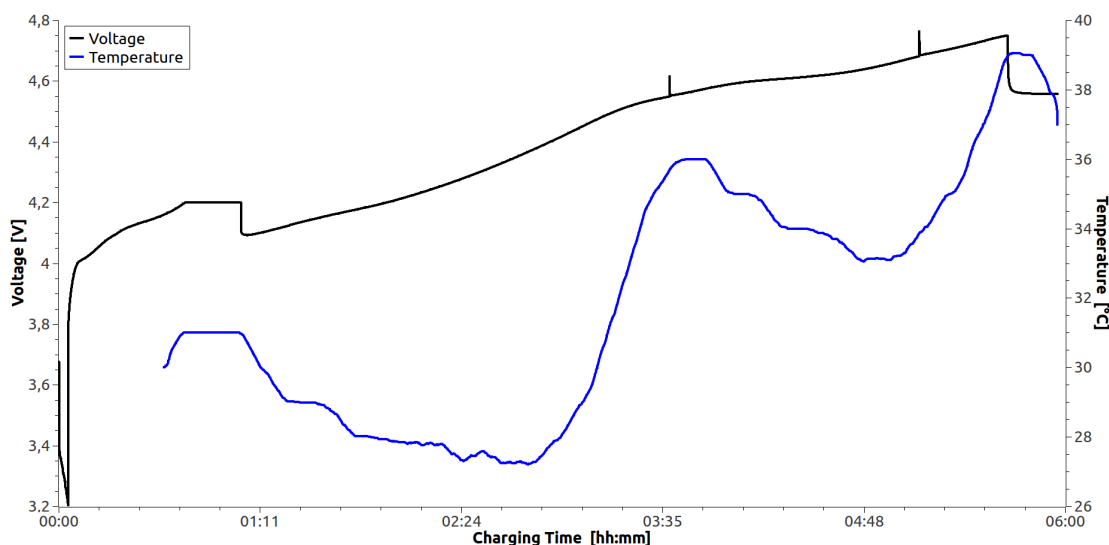


FIGURE 3.7: Development of the charging voltage and cell temperature (smoothed) during the overcharge of the BPC. The steps in the temperature curve result from the temperature resolution of 1 °C of the digital thermometer.

temperature low. A higher number of repetitions of the experiment could clarify this. In this second experiment the onset of the two stages of gas evolution were identified at 4.43 V and 4.71 V which is close to the values of the previous experiment. For most compounds the evolution starts slowly at the first stage with a small step followed by a plateau and the main amount is recorded at the higher voltage. Exceptions are  $\text{CO}_2$  and  $\text{SiF}_2(\text{CH}_3)_2$  which show already a large increase at 4.43 V and then a second rise after 4.71 V.  $\text{SiF}_2(\text{CH}_3)_2$  is probably a product of generated HF reacting with the column material and was usually found in the chromatogram as a broad, strongly tailing peak starting around 7.5 min. Upon ending the charging program the open circuit voltage returns to  $\sim 4.55$  V and the cell is cooling down. The gas evolution is slowly decreasing after the current flow stops and the signal decrease rate of the respective gases scales approximately with their retention time in the chromatogram, i.e. their volatility. While the emissions of permanent gases ceases rather fast, the signals of higher boiling compounds decrease only slowly. The decrease of gas evolution after the charging stopped can be attributed on one hand to the stop of electrochemical reactions and on the other hand to the decrease in temperature which may initiate some reactions but also raises the vapour pressure of the analytes.

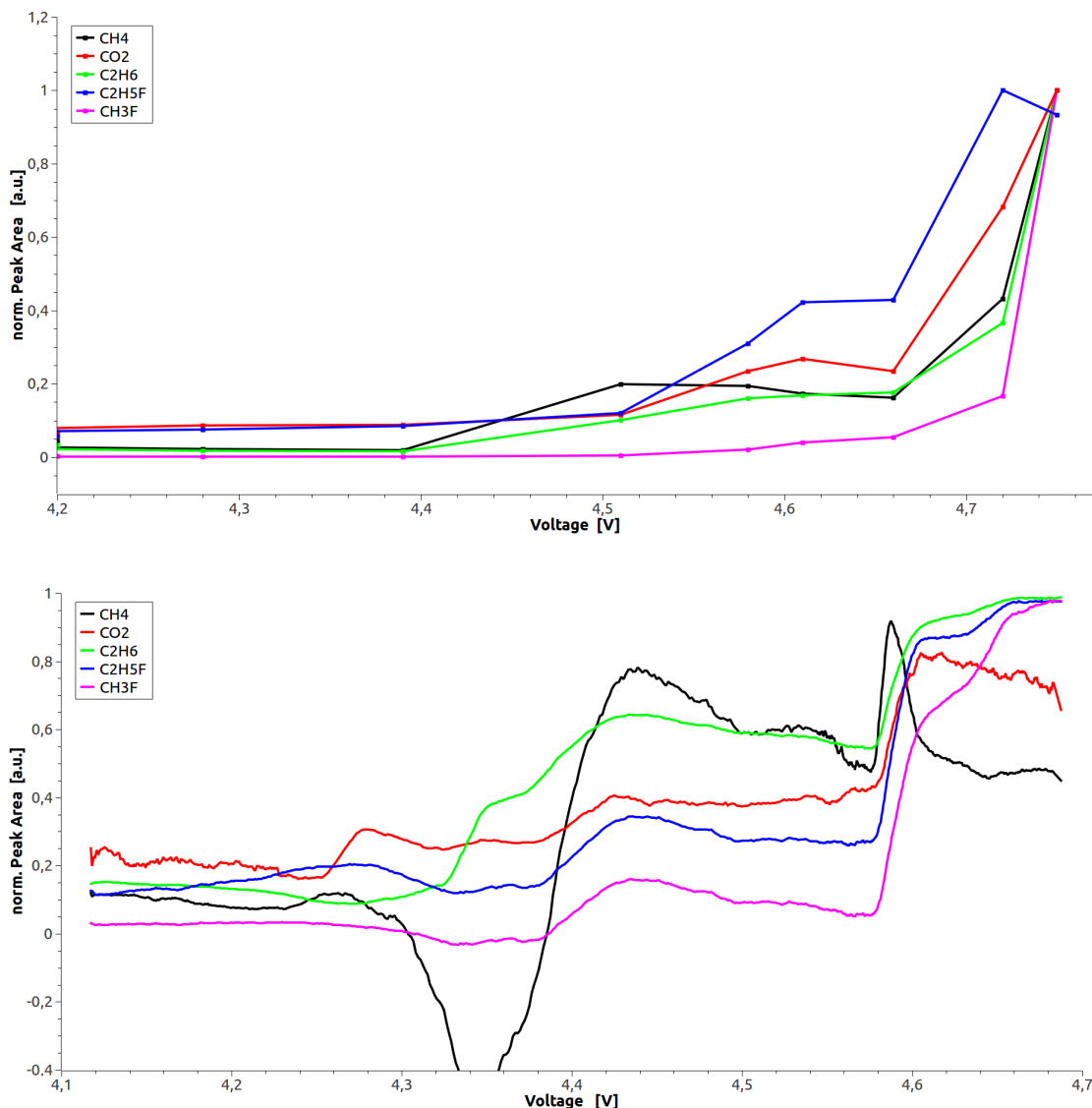


FIGURE 3.8: Signal for different gases from GC/MS (top) and FTIR (bottom) during the BPC overcharge. Note the different scales of the abscissae.

### 3.2.2 Gas evolution from coin cells

To characterise the stability limit and the origin of the decomposition products different electrolyte compositions were characterised by cyclic voltammetry (CV) in the ECC-DEMS cell setup with either glassy carbon (GC) or  $\text{LiCoO}_2$  working electrodes (as described in 2.1.2). Cyclic voltammetry was performed in a two-electrode setup, with the reference lead connected to the Li-counter electrode, since the construction of the measurement system did not allow a third electrode. The two-electrode setup and the equal area of working electrode and counter electrode can be sources of error in the



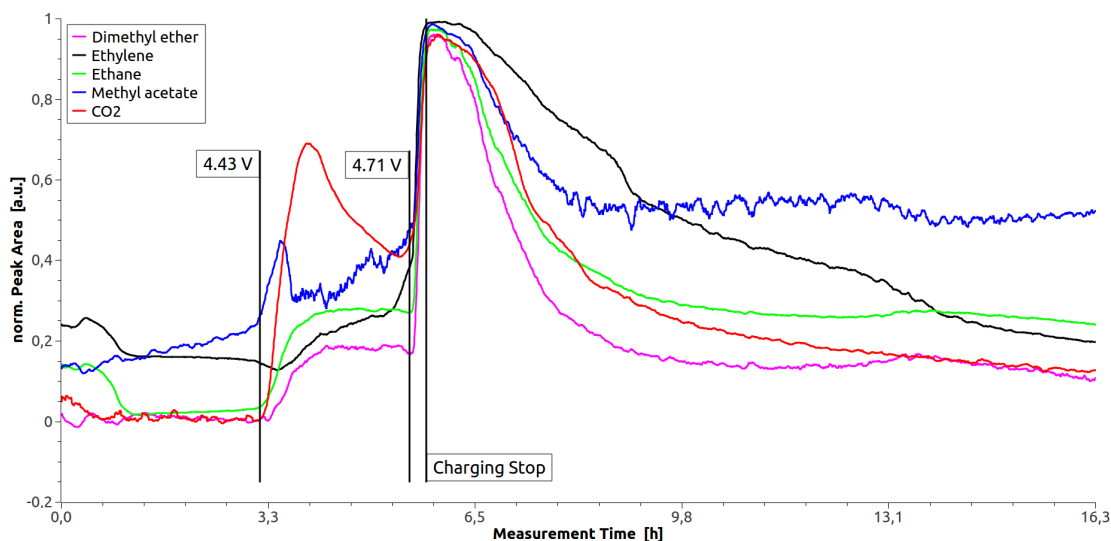


FIGURE 3.9: FTIR signal for the evolution of several gaseous compounds during the BPC overcharge.

measurement, but up to now it was not possible to construct a different geometry. This should be kept in mind during the evaluation of the results. The working electrode was cycled from the open circuit potential up to 8.0 V with a scan rate of 3.33 mV/min. Faster scan rates resulted in strong fluctuations of the current-voltage curve, which may be attributed to the drawbacks of the two-electrode setup or strong gas evolution at the electrode surface. It was also possible to obtain a rather high resolution of the GC/MS results concerning the potential with this small scan rate. Special attention was paid to avoid the drying-out of the coin cell since the constant gas purging leads to an increased evaporation of the electrolyte.

### 3.2.2.1 Glassy Carbon Electrodes

The 1 M solutions of  $\text{LiPF}_6$  in DMC, EC and DMC/EC (LP30) were examined with glassy carbon working electrodes. Unfortunately the sampling setup introduces air in the chromatogram which prevents the measurement of oxygen or water evolution and decreases the sensitivity for CO which coelutes. Table 3.5 lists the compounds measured from the oxidation of DMC, EC and DMC/EC on glassy carbon electrodes. The cyclic voltammograms of DMC, EC and DMC/EC are shown in Figure 3.10 and the onset potentials of the decomposition reactions, determined via the tangent method, are 6.54 V, 6.27 V and 6.14 V, respectively. It should be noted that a small peak was detected at 5.6 V for EC, but no gas evolution could be attributed to this potential. As expected for

volatile gaseous oxidation products the cyclic voltammograms show no cathodic peak of the reverse reactions.

Comparing the cyclic voltammogram to the gas evolution (Figure 3.11) —  $\text{CO}_2$  being taken here as a representative example — reveals that the gas evolution follows the "decomposition" current closely. As in the cyclic voltammogram the gas evolution for DMC shows a distinct peak while for EC only a slow increase with no maximum is observed and the signal for DMC/EC could be interpreted as a simple superposition of both curves. Similarly to the CV also in Figure 3.11 the amount of gas evolution is the highest in DMC followed by DMC/EC and finally pure EC. The question arises whether the decomposition reactions of DMC and EC follow a different mechanism. The distinct peak of DMC at a particular potential indicates an electrochemical reaction. The decomposition of EC may be caused by a chemical reaction which is initiated by an intermediate compound. A second plausible hypothesis is that the oxidation of EC leads to the formation of insoluble compounds — compare section 1.3.2, (1.35) — which form a passivating layer on the electrode surface and attenuate further reaction. It should be noted that the surface of the glassy carbon electrodes was found to have a brownish discolouration as it was retrieved after all experiments. The different behaviour could also be attributed to the lower stability of DMC or may be a kinetic effect caused by the lower viscosity of DMC. The earlier on-set of decomposition for EC and DMC/EC are contradicting the former. These on-set potentials are in contradiction to literature values (Table 1.3) where a higher stability of EC is reported. To elucidate this behaviour in more detail further experiments are required. Within the scope of this thesis the experiments involving the coin cells could only be conducted once each. Traces of EC were found also in the chromatogram of the DMC electrolyte. They are suspected to originate from EC trapped in the gas sampling apparatus during earlier experiments.

On comparison of the evolution of various gases over time it was observed that the signals of nearly all compounds rise and fall simultaneously (Figure 3.12). Similar behaviour was found for all electrolyte compositions. The appearance of the products starting at a single potential suggests that the formation of decomposition products is initiated by a single reaction of the electrolyte. Following this assumption of an initiating reaction, whose products take part in several reaction pathways, one may expect the detection of secondary products with different time delays according to their formation rate. However, on the rather slow time scale of the conducted experiments this was not

observed.

Exceptions were found for analytes like methanol and the unidentified compounds detected from DMC with retention times of 10.96 min and 11.22 min which showed a delayed signal compared to ethane and also the decrease of the peak had no clear trend. The fluctuations in the methanol curve are probably due to the low amount detected, which leads to a noisy signal — a phenomenon that was observed also with other compounds of low abundance. A possible explanation for the delayed appearance of these compounds is offered from a comparison with the corresponding chromatogram (cf. Figure 3.13). The delay appears to increase along with the retention time of the compounds. Low volatility or high solubility of the compounds in the electrolyte could be responsible for this effect as it would shift the release of the compounds from the electrolyte to higher concentrations i.e. to a later time.

TABLE 3.5: Compounds identified by GC/MS during cyclic voltammetry of  $\text{LiPF}_6$  in DMC, EC and DMC/EC. X marks identified compounds.

Compound (RT/min)	DMC	EC	DMC/EC
CO (1.40)	X	X	X
CO <sub>2</sub> (1.81)	X	X	X
Methane (1.49)	X		X
Ethylene (2.48)		X	X
Ethane (2.97)	X	X	X
Propane (5.77)	X		
Butane (8.03)	X		
Fluoro methane (2.23)	X		X
Difluoro methane (2.80)	X		X
Trifluoro methane (2.33)		X	
Fluoro ethane (5.04)	X		X
1,1-difluoro ethane (5.27)	X	X	X
2-fluoro propane (7.10)	X		
Methanol (6.50)	X		
Dimethyl ether (6.26)	X		
Dimethoxy methane (9.50)	X		
Methyl formate (7.54)	X		X
Methyl acetate (9.42)	X		X
Acetaldehyde (6.84)		X	
EMC (12.85)			X
SiF <sub>2</sub> (CH <sub>3</sub> ) <sub>2</sub> (7.56)	X	X	X

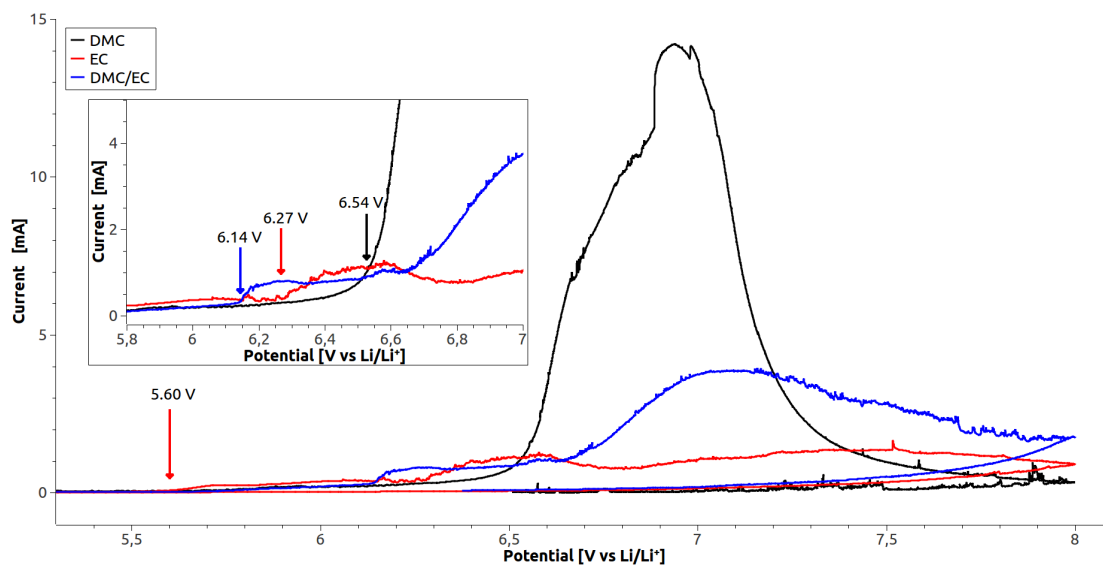


FIGURE 3.10: Cyclic voltammogram of the DMC, EC and DMC/EC electrolytes on GC. Onset potentials marked by arrows. Inset: Detail of the onset region.

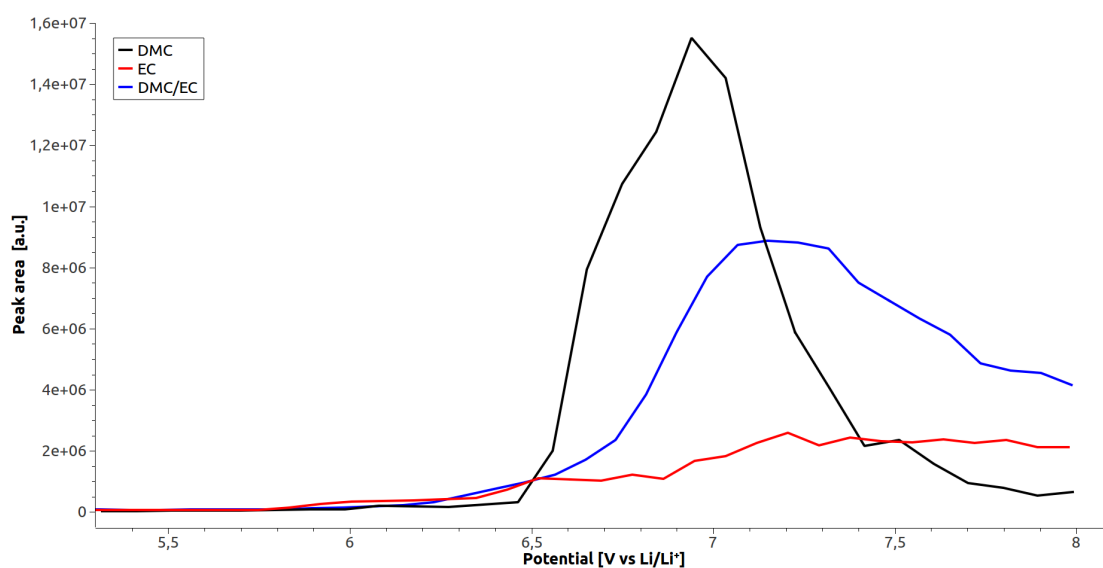


FIGURE 3.11: CO<sub>2</sub> signal recorded during the cyclic voltammetry of DMC, EC and DMC/EC on glassy carbon.

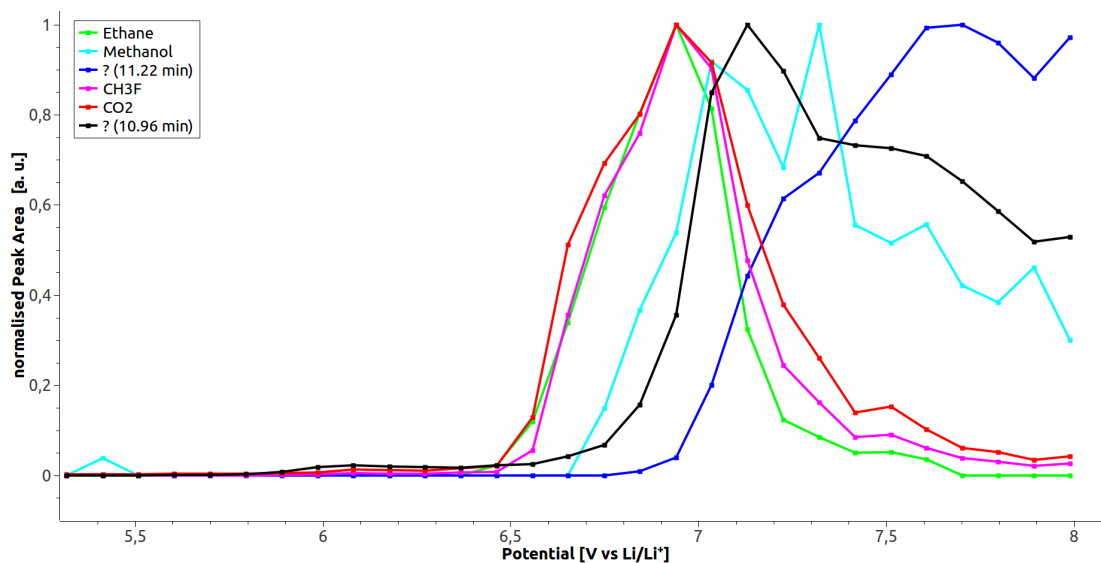


FIGURE 3.12: GC/MS signals for several gases during the cyclic voltammetry of DMC on a glassy carbon electrode.

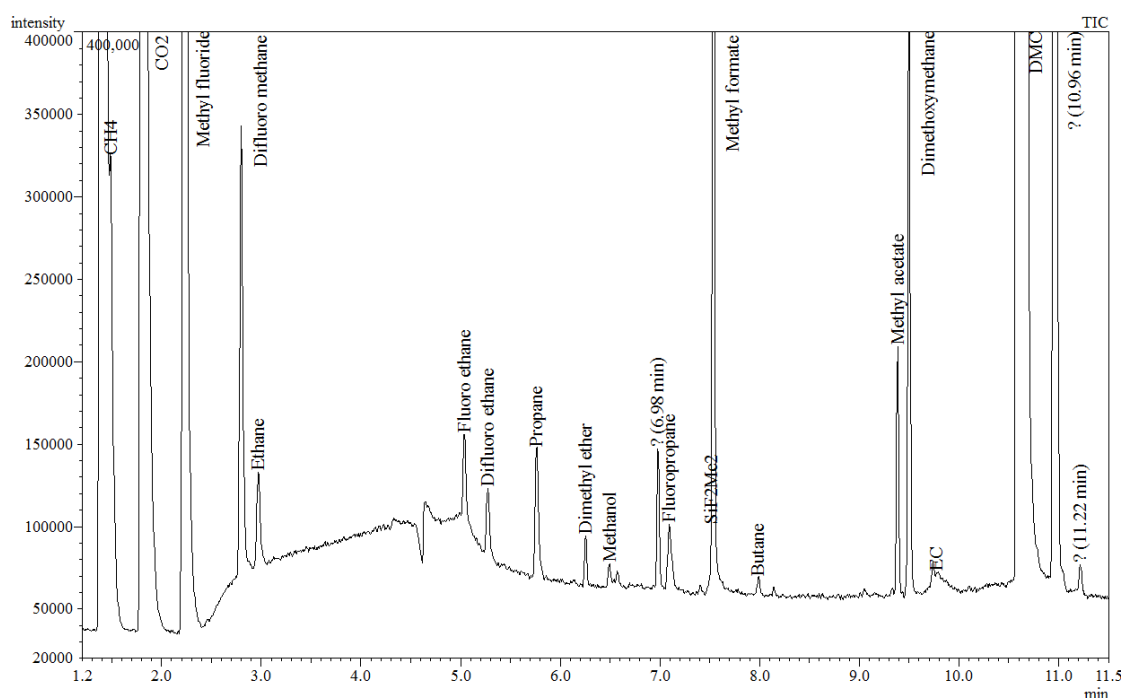


FIGURE 3.13: Gas chromatogram recorded at a potential of 6.92 V from DMC on a glassy carbon electrode.

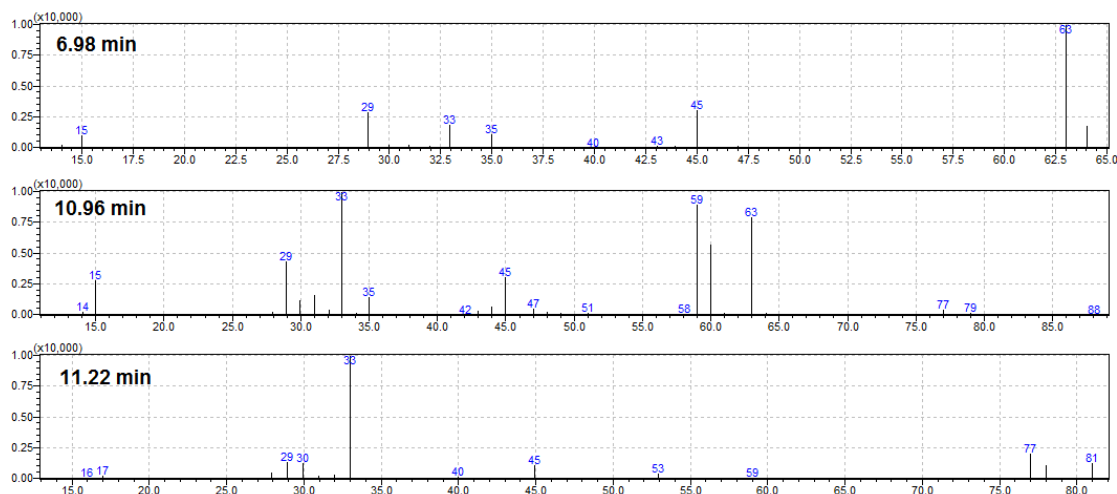


FIGURE 3.14: Mass spectra of unidentified compounds from DMC decomposition on a glassy carbon electrode.

### 3.2.2.2 Formation Pathways of the Compounds

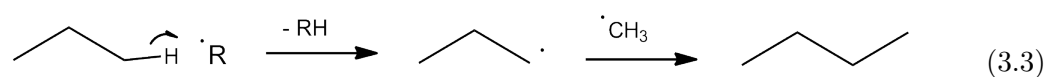
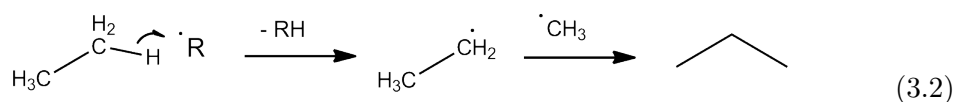
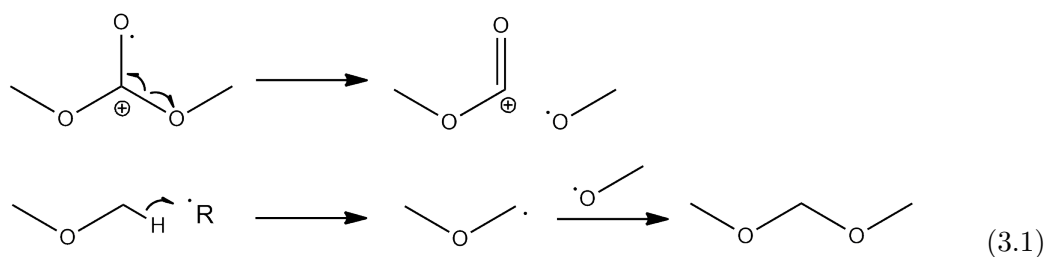
Most of the compounds detected during the oxidation of the solvents are consistent with the findings reported in literature (cf. section 1.3.2). However, in contrast to the light hydrocarbons and  $\text{CO}_2$  the detection of substances like methyl acetate under "oxidative" conditions, i.e. high potentials at the working electrode, has not been reported yet. A possible explanation is that they are formed simultaneously through reduction at the anode (i.e. the counter electrode). Especially with the two-electrode setup used, which resembles a battery, this seems likely. The gas analysis method does not distinguish the location of gas formation. Based on this assumption the following hypothesis can be suggested in concordance with the results of Table 3.5. If this assumption is correct, most compounds are formed at the anode side.

The formation of most analytes can be explained from the reactions given in section 1.3. Based on the compounds that were detected from the different electrolyte compositions, the reactions reported in literature and the origin of the decomposition compounds were evaluated for their plausibility. The conclusions are summarised in Table 3.6.

Although further experimental evidence is indispensable, the following reactions are assumed to be plausible for the compounds dimethoxy methane (3.3), propane (3.2) and butane (3.1), whose formation has not been clarified yet. Unfortunately no explanation has been found for the formation of  $\text{CHF}_3$ ,  $\text{CH}_2\text{F}_2$ , 1,1-difluoro ethane and 2-fluoro propane.

TABLE 3.6: Compounds identified by GC/MS during cyclic voltammetry of  $\text{LiPF}_6$  in DMC. Assigned according to the suspected precursor and formation mechanism. R: Reductive (i.e. at the anode), O: Oxidative (i.e. at the cathode), T: thermally induced, ?: unclear.

Compound	DMC	EC
CO	R & O	R & O
$\text{CO}_2$	R & O	R & O
Methane	R	
Ethylene		R
Ethane	R	?
Fluoro methane	T	
Fluoro ethane	T ?	
Methanol	R	
Dimethyl ether	R	
Methyl formate	R	
Methyl acetate	R	
Acetaldehyde		O



### 3.2.2.3 $\text{LiCoO}_2$ Electrodes

As the glassy carbon (GC) electrodes are considered inert electrodes and not comparable with the cathode material used in LIBs the cyclic voltammetry experiment of the DMC/EC electrolyte was repeated with a  $\text{LiCoO}_2$  working electrode obtained from *Pi-Kem*. Comparison of the cyclic voltammograms (Figure 3.15) of GC and  $\text{LiCoO}_2$  shows quite some difference in the electrochemical behaviour. The onset of the anodic peak starts at 4.0 V on  $\text{LiCoO}_2$  in contrast to 6.1 V on GC. The 4.0 V are consistent with the

Li-deintercalation from the  $\text{Li}_{1-x}\text{CoO}_2$  electrode. This is corroborated by the analysis of the gas evolution with respect to the current signal in the cyclic voltammetry (Figure 3.16). The gas evolution does not start until 6.2 V and one could conclude that in the cyclic voltammogram the peaks from Li-deintercalation and electrolyte decomposition overlap.

The actual anodic peak currents for GC and  $\text{LiCoO}_2$  are 3.8 mA and 245 mA, respectively. While the electrode surface of the smooth GC electrode is easily calculated from the macroscopic dimensions a far greater specific surface has to be expected for the porous  $\text{LiCoO}_2$  electrode. Unfortunately, it was not possible to distinguish whether the current increase resulted from an electrochemical reaction of the cathode material itself, the larger surface area or an catalytic effect of the cathode material on the electrolyte decomposition. The cathode was examined afterwards by X-ray powder diffraction for evidence of a  $\text{LiCoO}_2$ -decomposition resulting in  $\text{O}_2$  release (1.55), but no proof of newly formed phases was found.

On comparing the evolved gases with either GC or  $\text{LiCoO}_2$  used as electrode materials, it is interesting to note the different product range (Table 3.7). While CO,  $\text{CO}_2$  and light hydrocarbons were detected from the glassy carbon and the  $\text{LiCoO}_2$  electrodes no fluorine containing compounds were found with  $\text{LiCoO}_2$  except minor traces of  $\text{CH}_3\text{F}$  and  $\text{CHF}_3$ . Instead the generated amounts of ethane, propane and butane increased drastically. The formation of  $\text{CH}_3\text{F}$ , the prevalent fluorine containing compound on glassy carbon, is strongly suppressed on  $\text{LiCoO}_2$  (Figure 3.17). This has not been reported up to now. Two hypotheses have been found to explain the effect of  $\text{LiCoO}_2$  on the gas evolution. As the amount of fluorine containing compounds was highly reduced, one could assume that a reaction involving the cathode material traps or depletes fluorine, so that it is not available for other reactions. It seems also possible that the presence of  $\text{LiCoO}_2$  facilitates a particular reaction so that it is favoured compared to the reactions generating fluorine containing gases. The obtained results demonstrate that it is not sufficient to extrapolate findings from one system to another, as the processes are still not understood well enough.

Also the formation of EMC is much more favoured on  $\text{LiCoO}_2$ . All compounds detected follow the same trend as  $\text{CO}_2$  and show two stages in the gas evolution curve, where the first one begins around 6.3 V and the second one around 7.2 V, (Figure 3.16) in contrast to the results on glassy carbon electrodes (Figure 3.11, Figure 3.12). No apparent change in the gas evolution at the second stage indicates the beginning of a different process.



However, the fluctuations in the current signal could indicate that the cell was about to dry out — probably due to a depletion of the electrolyte. Around 7.75 V the experiment stopped as the cell lost internal contact.

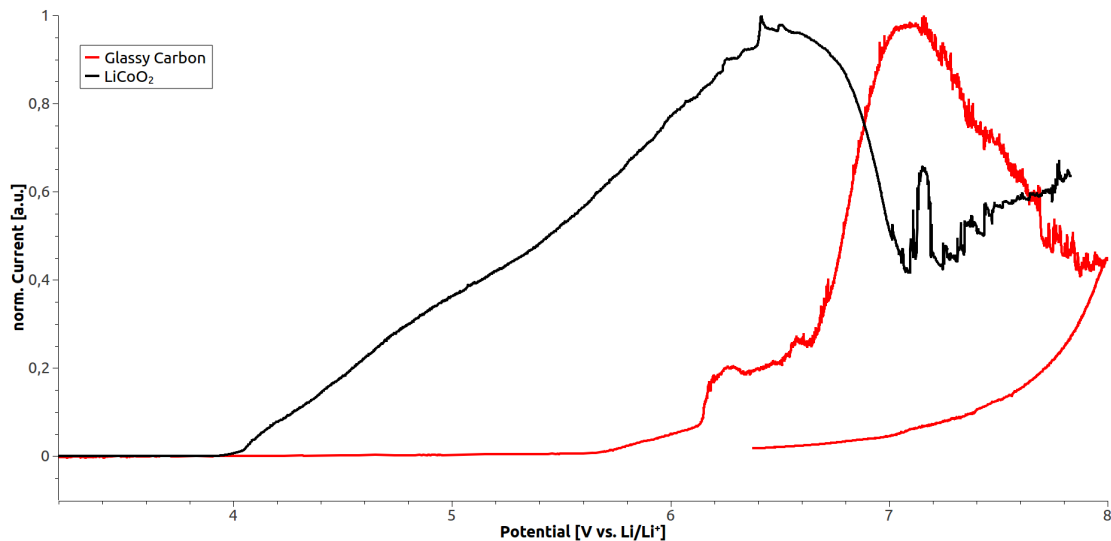


FIGURE 3.15: Cyclic voltammetry curves of DMC/EC with glassy carbon and  $\text{LiCoO}_2$  working electrodes. Current normalised for comparison.

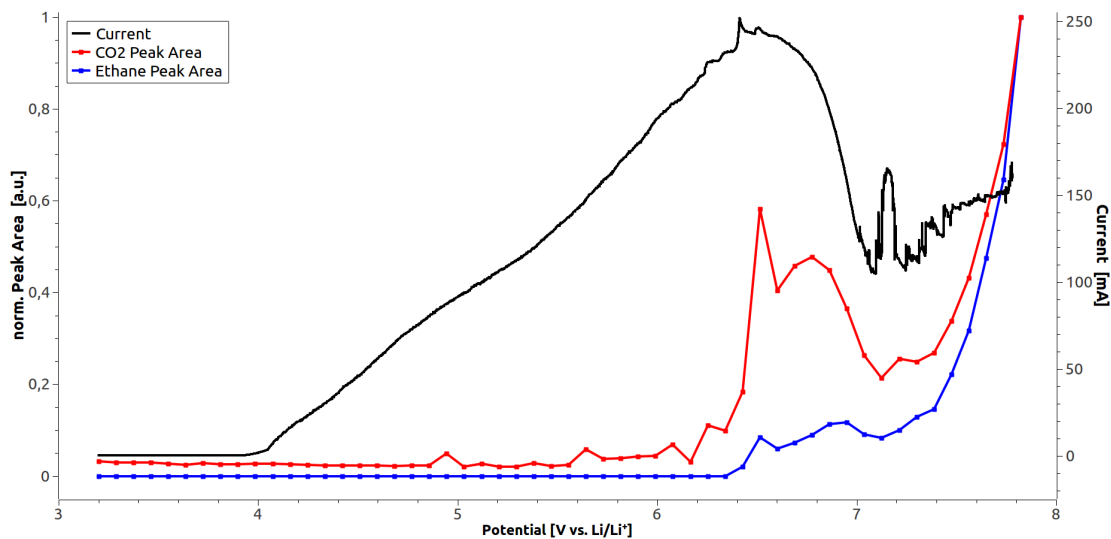


FIGURE 3.16: Cyclic voltammetry curve and GC/MS signals for  $\text{CO}_2$  and ethane on  $\text{LiCoO}_2$ .

TABLE 3.7: Compounds identified by GC/MS during cyclic voltammetry of  $\text{LiPF}_6$  in DMC/EC on glassy carbon and  $\text{LiCoO}_2$  electrodes. X corresponds to identified compounds. ? correspond to the unidentified compounds described in Figure 3.14

Compound (RT/min)	Glassy Carbon	$\text{LiCoO}_2$
CO (1.40)	X	X
$\text{CO}_2$ (1.81)	X	X
Methane (1.49)	X	X
Ethylene (2.48)	X	X
Ethane (2.97)	X	X
Propane (5.77)		X
Butane (8.03)		X
Fluoro methane (2.23)	X	X
Difluoro methane (2.80)	X	
Trifluoro methane (2.33)		X
Fluoro ethane (5.04)	X	
1,1,-difluoro ethane (5.27)	X	
Methanol (6.50)	X	
Dimethyl ether (6.26)	X	X
Methyl formate (7.54)	X	X
Methyl acetate (9.39)	X	X
EMC	X	X
Ethyl methyl ether (8.81)		X
$\text{SiF}_2(\text{CH}_3)_2$ (7.56)	X	X
? (10.96)	X	X

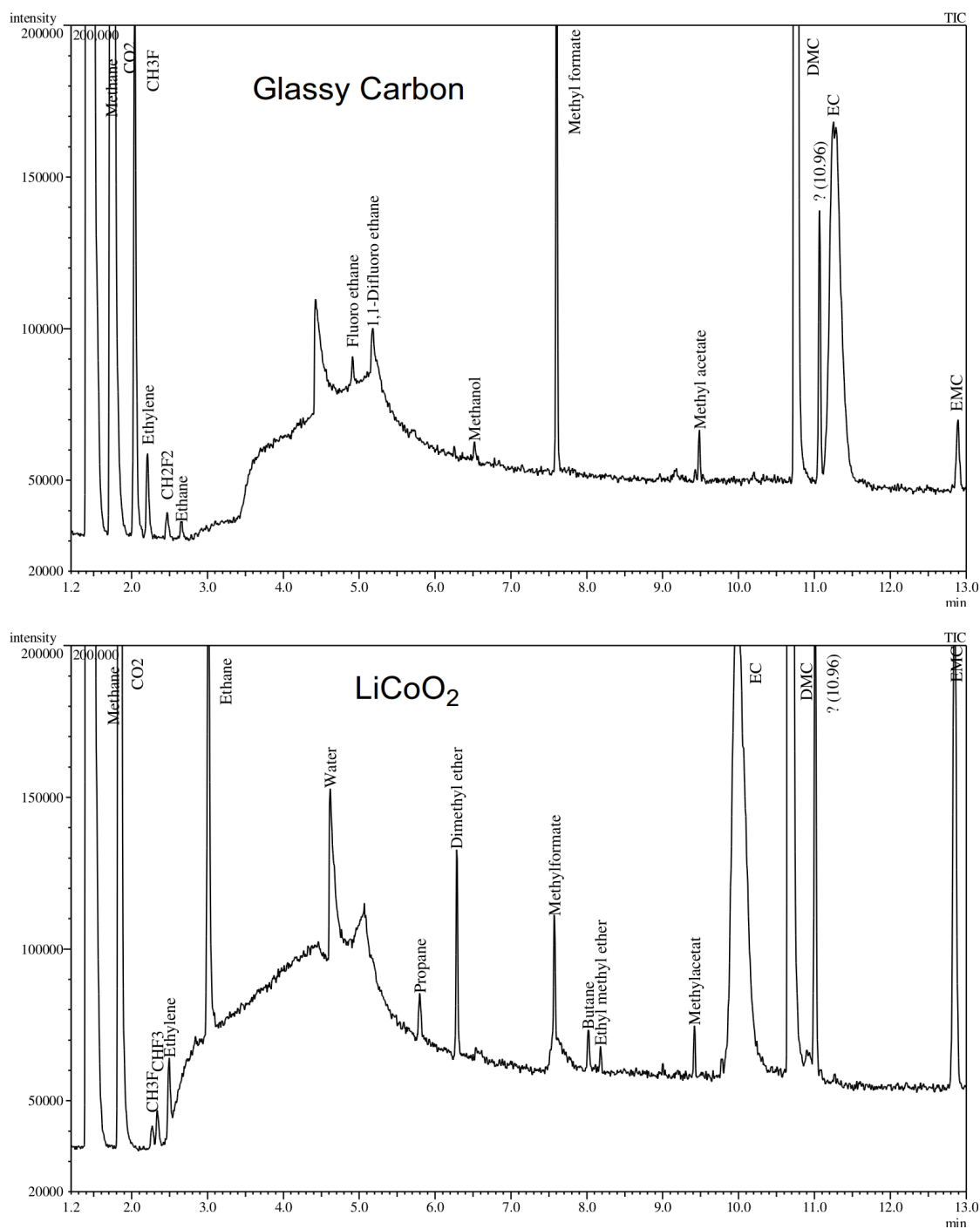


FIGURE 3.17: Gas chromatograms of DMC/EC on glassy carbon (top) and LiCoO<sub>2</sub> (bottom). The retention times in the upper chromatogram are shifted as the oven program was slightly changed.



## Chapter 4

# Conclusions

The goal of this work was to develop a new method for the characterisation of gas evolution from lithium ion batteries. It was a particular objective of this work to develop a method that allows the analysis of evolved gases with high time resolution, as this may change within only few minutes during fast processes in the cell.

After a period of trial, where several setups had been tested, a method was established, based on the combination of GC/MS and FTIR, which allows the detection of volatile compounds released from LIBs. The high sensitivity of the GC/MS instrument enables the identification and quantification of compounds over a wide range of concentrations and the coupling with the FTIR spectrometer provides the ability to monitor the concentration changes with a resolution below 30 seconds. The unique identification capabilities of the GC/MS make it possible to analyse battery behaviour in a single experiment as identification and quantification are done simultaneously and the multivariate data analysis and modelling of the FTIR data can be performed after the experiment. Two different gas sampling cells allow the analysis of coin cells and commercial LIBs, which makes the method valuable for research and development as well as industrial battery testing. Especially the detection of the small gas volumes released from coin cells is a noticeable achievement. So far the detection of decomposition products is only possible in a semi-quantitative manner. Generally, a more reliable way of quantification can be implemented, as will be illustrated later on.

As the method was established several experiments were conducted to evaluate the method. The results of these experiments reveal its versatility. During the overcharge of a commercial cell the generated gases were identified and their evolution over time

was monitored in detail. Two stages of gas evolution were observed which are presumed to correspond to two different decomposition processes. Furthermore, the behaviour of different electrolyte compositions was studied in coin cells by cyclic voltammetry on inert working electrodes and typically used battery electrodes. Based on the findings and published literature data a scheme was formulated that proposes possible formation pathways of the analytes. It was also found that the material of the working electrode has a major impact on the amount and range of decomposition products.

The results are plausible and reasonable and agree to a large extent with literature. Since most experiments could only be conducted once, they have to be supported by additional measurements to ensure the validity of the data.

Although the basic method is now established, there is still room for improvement, especially concerning the quantification, time resolution and the PLS model. To improve the quantification ability different approaches are conceivable: By mixing the purge gas with an internal standard gas, the comparison between experiments could be improved. A small, constant concentration of an inert gas provides a steady reference which can be set in relation to the analyte signals and reduces fluctuations. A possibility to increase the sensitivity of the GC/MS is to install a trap concentrator in which the analytes, that normally go to waste during the GC/MS runs, are adsorbed and then released and injected at once. It would also be a great improvement of the method if the speed of the GC/MS runs could be improved further. Besides an optimised temperature and flow program, new techniques like the *vacuum outlet technique* could reduce analysis times tremendously. Furthermore the partial least squares regression model could potentially be improved even more. It has weaknesses to distinguish compounds with similar infrared spectra and still shows some fluctuations, especially when the concentrations of the analytes are low. The design of an improved gas sampling chamber for commercial cells from more resistant materials would provide more safety and access to more severe testing conditions.

# Bibliography

- [1] M. S. Whittingham, *Chem. Rev.* **2004**, *104*(10), 4271–4302.
- [2] M. S. Whittingham, *Science* **1976**, *192*, 1126–1127.
- [3] J. Besenhard, H. Fritz, *J. Electroanal. Chem.* **1974**, *53*, 329–333.
- [4] J. Besenhard, *Carbon* **1976**, *14*, 111–115.
- [5] K. Xu, *Chem. Rev.* **2004**, *104*(10), 4303–4417.
- [6] D. Seetharaman, Tesla ceo defends electric cars after battery fire, **2013**, URL <http://www.reuters.com/article/2013/10/04/us-autos-tesla-fire-idUSBRE9920SX20131004>, accessed: 27.04.2014.
- [7] D. Guyomard, J. Tarascon, *Adv. Mater.* **1994**, *6*(5), 408.
- [8] R. Liu, J. Duay, S. Lee, *Chem. Comm.* **2011**, *47*(5), 1384–1404.
- [9] P. G. Bruce, *Chem. Comm.* **1997**, 1817–1824.
- [10] J. Bergveld, W. Kruijt, P. Notten, *Battery Management Systems: Design by Modelling*, Springer Science+Business, New York, **2002**, 34ff.
- [11] S. Anthony, Rice university creates spray-on, paint-based lithium-ion batteries, URL <http://goo.gl/nzqZru>, accessed: 16.06.2014.
- [12] Cost reduction for secondary lithium-ion battery, URL [http://www.aist.go.jp/aist\\_e/latest\\_research/2004/20041203/20041203.html](http://www.aist.go.jp/aist_e/latest_research/2004/20041203/20041203.html), accessed: 16.06.2014.
- [13] K. Kumai, H. Miyashiro, Y. Kobayashi, K. Takei, R. Ishikawa, *J. Power Sources* **1999**, *81-82*, 715–719.
- [14] M. Doeff, *Batteries for Sustainability*, Springer, New York, **2013**, 9ff.

- [15] A. Manthiram, *Lithium Batteries-Science and Technology*, Springer Science+Business, New York, **2003**, 3ff.
- [16] A. Holleman, N. Wiberg, *Lehrbuch der Anorganischen Chemie*, de Gruyter, Berlin, Germany, **2007**, 102nd ed., 1260.
- [17] M. Ishikawa, M. Morita, *Lithium Batteries-Science and Technology*, Springer Science+Business, New York, **2003**, 297ff.
- [18] M. Winter, K.-C. Moeller, J. Besenhard, *Lithium Batteries-Science and Technology*, Springer Science+Business, New York, **2003**, 144ff.
- [19] P. Verma, P. Maire, P. Novak, *Electrochim. Acta* **2010**, *55*, 6332–6341.
- [20] J. Zhang, *Batteries for Sustainability*, Springer, New York, **2013**, 471ff.
- [21] S. Santhanagopalan, Z. Zhang, *Batteries for Sustainability*, Springer, New York, **2013**, 135ff.
- [22] M. Morita, T. Shibata, N. Yoshimoto, M. Ishikawa, *Electrochim. Acta* **2002**, *47*, 2787–2793.
- [23] D. Guyomard, J. Tarascon, *J. Electrochem. Soc.* **1993**, *140*(11), 3071–3081.
- [24] M. Ishikawa, M. Morita, *Lithium Batteries-Science and Technology*, Springer Science+Business, New York, **2003**, 530ff.
- [25] X. Zhang, R. Kostecki, T. J. Richardson, J. K. Pugh, P. N. J. Ross, *J. Electrochem. Soc.* **2001**, *148*(12), 1341–1345.
- [26] K. Hayashi, Y. Nemoto, S. Tobishima, J. Yamaki, *Key Eng. Mater* **1999**, *157-158*, 273–280.
- [27] K. Xu, S. P. Ding, T. R. Jow, *J. Electrochem. Soc.* **1999**, *146*, 4172–4178.
- [28] D. Aurbach, A. Schechter, *Lithium Batteries-Science and Technology*, Springer Science+Business, **2003**, 554.
- [29] M. Moshkovich, M. Cojocaru, H. Gottlieb, D. Aurbach, *J. Electrochem. Soc.* **2001**, *497*, 84–96.
- [30] M. Ue, *Lithium-Ion Batteries: Science and Technologies*, Springer, New York, **2009**, 75ff.



- [31] L. Xiao, X. Ai, Y. Cao, H. Yang, *Electrochim. Acta* **2004**, *49*, 4189–4196.
- [32] B. Barnett, D. Ofer, S. Sriramulu, R. Stringfellow, *Batteries for Sustainability*, Springer, New York, **2013**, 285ff.
- [33] M. Egashira, H. Takahashi, S. Okada, J. Yamaki, *J. Power Sources* **2001**, *92*, 267–271.
- [34] M. Arakawa, J.-I. Yamaki, *J. Power Sources* **1995**, *54*, 250–254.
- [35] W. Kong, H. Li, X. Huang, L. Chen, *J. Power Sources* **2005**, *142*, 285–291.
- [36] G. Gachot, P. Ribiere, D. Mathiron, S. Grugeon, M. Armand, J.-B. Leriche, S. Pilard, S. Laruelle, *Anal. Chem.* **2011**, *83*, 478–485.
- [37] T. Ohsaki, T. Kishi, T. Kuboki, N. Takami, N. Shimura, Y. Sato, M. Sekino, A. Satoh, *J. Power Sources* **2005**, *146*, 97–100.
- [38] T. Sasaki, T. Abe, Y. Iriyama, M. Inaba, Z. Ogumi, *J. Power Sources* **2005**, *150*, 208–215.
- [39] G. Gachot, S. Grugeon, M. Armand, S. Pilard, P. Guenot, J. Tarascon, S. Laruelle, *J. Power Sources* **2008**, *178*, 409–421.
- [40] H. Yoshida, T. Fukunaga, T. Hazama, T. Terasaki, M. Terasaki, M. Mizutani, M. Yamachi, *J. Power Sources* **1997**, *68*, 311–315.
- [41] E. Roth, C. Crafts, D. Doughty, J. McBreen, Sandia report - thermal abuse performance of 18650 li-ion cells, Sandia National Laboratories, Albuquerque, NM, USA, **2004**, 129ff.
- [42] T. Kawamura, A. Kimura, M. Egashira, S. Okada, J. Yamaki, *J. Power Sources* **2002**, *104*, 260–264.
- [43] G. Gachot, S. Grugeon, I. Jimenez-Gordon, G. Eshetu, S. Boyanov, A. Lecocq, G. Marlair, S. Pilard, S. Laruelle, *Anal. Methods* **2014**, *6*, 6120–6124.
- [44] S. J. Ashton, *Design, Construction and Research Application of a Differential Electrochemical Mass Spectrometer (DEMS)*, Springer, Berlin, Heidelberg, Germany, **2012**, 9ff.

- [45] J. Vetter, M. Holzapfel, A. Wuersig, W. Scheifele, J. Ufheil, P. Novak, *J. Power Sources* **2006**, *159*, 277–281.
- [46] M. Holzapfel, A. Wuersig, W. Scheifele, J. Vetter, P. Novak, *J. Power Sources* **2007**, *174*, 1156–1160.
- [47] H.-J. Huebschmann, *Handbook of GCMS-Fundamentals and Application*, Wiley-VCH, Weinheim, Germany, **2009**, 2nd ed.
- [48] B. Stuart, *Infrared Spectroscopy- Fundamentals and Applications*, John Wiley & Sons, Ltd, West Sussex, England, **2004**.
- [49] Data sheet: Swing 4400 rechargeable lithium-ion cell. boston power, westborough, ma, usa (2010), URL <http://liionbms.com/pdf/bostonpower/swing4400.pdf>, accessed: 25.04.2014.

## Appendix A

### Additional Figures

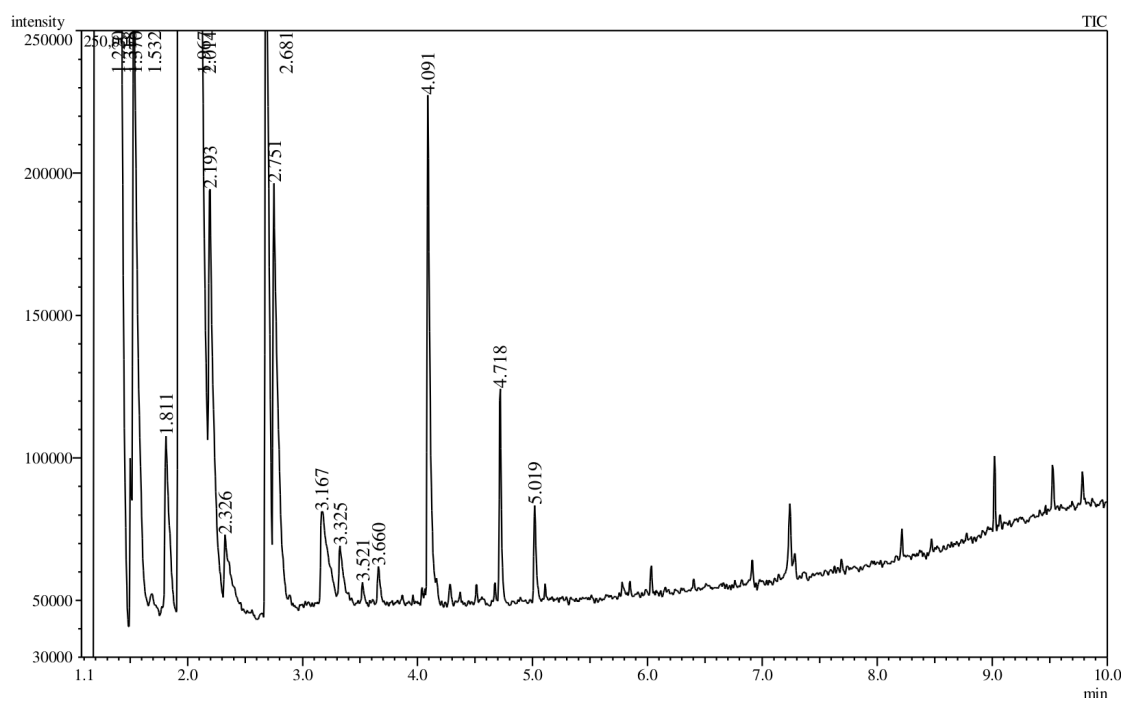


FIGURE A.1: Gas chromatogram of compounds detected from the separators during the preliminary experiments. Method A

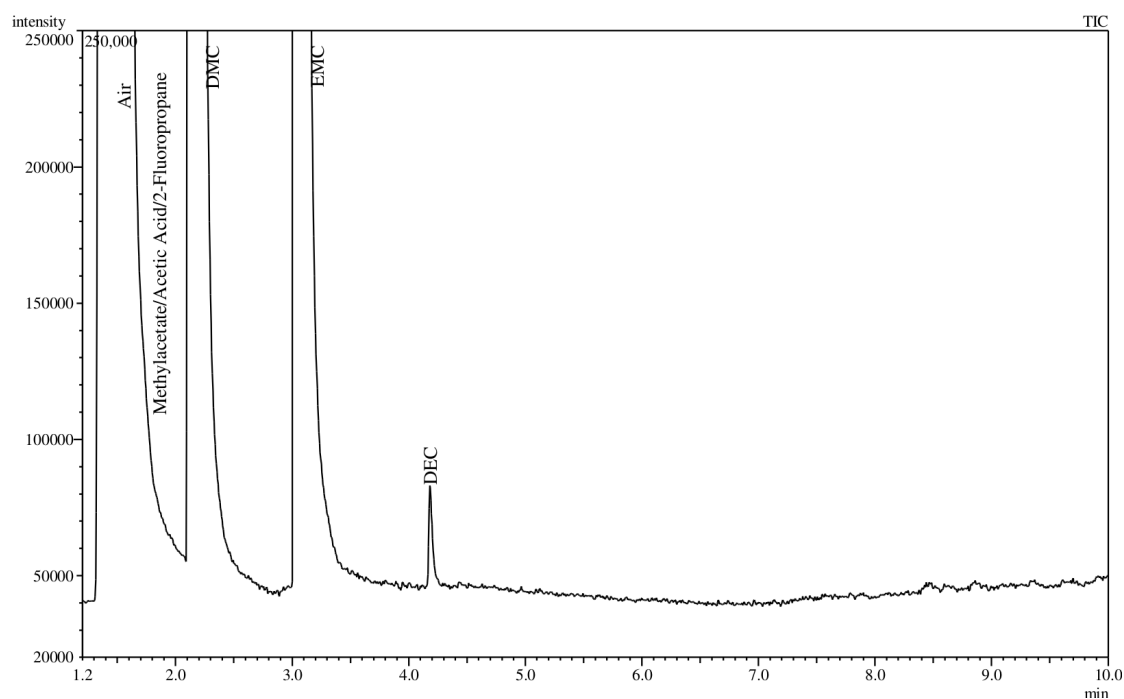


FIGURE A.2: Gas chromatogram recorded at a charging voltage of 4.2 V during cycling of the BPC in the normal range. Method B.

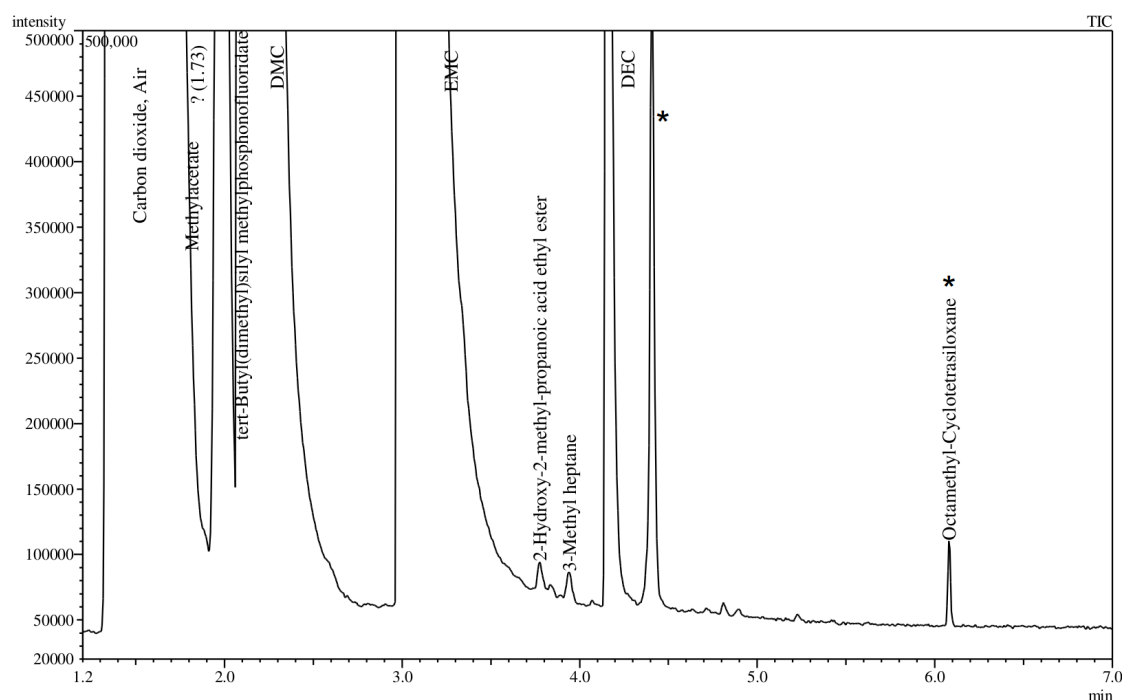


FIGURE A.3: Gas chromatogram recorded at 5.0 V during the non continuous over-charge of the BPC. Method B. \* marks column decomposition products.

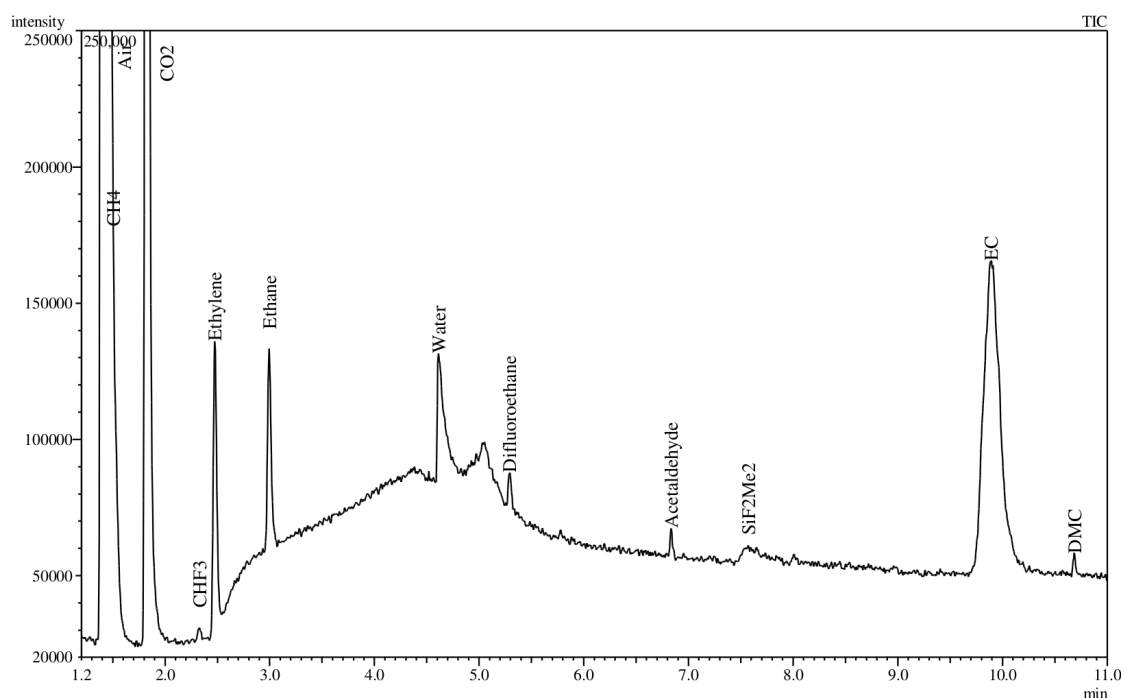


FIGURE A.4: Gas chromatogram recorded during the cyclic voltammetry of EC on glassy carbon at 7.4 V.

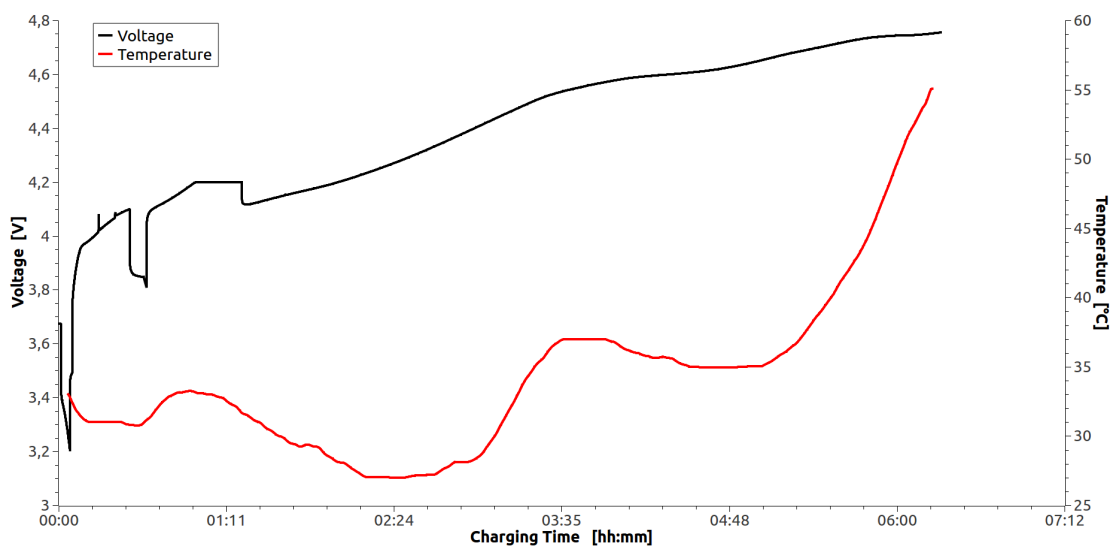


FIGURE A.5: Charging voltage and cell temperature during the first BPC continuous overcharge experiment.



# Appendix B

## Abstract (English)

The increasing demand for mobility and remotely available electric energy promotes the development of batteries with higher power and capacity. Lithium ion batteries (LIB) are currently the most successful technology to satisfy this demand in our daily life. At the same time the safety of LIBs has to be addressed as a high amount of energy is stored in these devices and several cases of battery failure are known, in which the uncontrolled release of this energy lead to an ignition or explosion of the cell. The flammability of the organic electrolytes which are in use in conventional LIBs and the release of flammable or toxic gases during battery failure have motivated many researchers to examine the decomposition processes in batteries. Up to now this has mainly been done by characterisation of the electrolyte degradation products after a controlled abuse of the cell.

In this work a new method was developed to characterise the gaseous emissions from LIBs with high time resolution during the process of battery failure. This was achieved by combining the analytical abilities of gas chromatography/mass spectrometry (GC/MS) and Fourier transform infrared spectroscopy (FTIR). A measuring station was constructed which allows the continuous monitoring of evolved gases via simultaneous analysis by GC/MS and FTIR. GC/MS allows the identification and quantification of analytes while FTIR monitors fast concentration changes with high time resolution. A partial least squares regression model was used to correlate the GC/MS data with the FTIR signal. This method was successfully applied to characterise the gas evolution from coin cells and commercial high power cells.

The volatile decomposition products from a commercial cell during controlled overcharge were identified and their release was monitored relative to the charging voltage.

Furthermore the gaseous compounds generated from different electrolyte compositions during a cyclic voltammetry experiment were identified and the stability of different electrolytes characterised. The influence of electrode materials was investigated by comparing the product spectrum and decomposition behaviour on an inert working electrode and a realistic battery cathode. Special attention was paid to the development process and the evaluation of the new method.



## Appendix C

### Abstract (German)

Die steigende Nachfrage nach Mobilität und Verfügbarkeit von elektrischer Energie ist Motivation für die Entwicklung von neuen Batterien mit höherer Leistung und Kapazität. Lithium Ionen Batterien (LIB) sind die derzeit erfolgreichste Technologie um diesen Bedarf im täglichen Leben zu decken. Mit der Entwicklung leistungsfähiger Batterien steigen auch die Sicherheitsanforderungen, da in ihnen eine hohe Energiemenge gespeichert ist und bereits mehrere Unfälle bekannt wurden, bei denen die unkontrollierte Freisetzung dieser Energie zur Entzündung und Explosion von Batterien geführt hat. Die hohe Entzündlichkeit der organischen Elektrolyte in handelsüblichen LIB und die Freisetzung von brennbaren oder giftigen Gasen während des Batterieversagens haben viele Wissenschaftler motiviert die Zersetzungsprozesse in LIB zu untersuchen. Bisher fand dies hauptsächlich durch die Analyse der Elektrolyt-Zersetzungsprodukte nach einer kontrollierten Überlastung der Batterie statt.

In dieser Arbeit wurde eine neue Methode zur zeitaufgelösten Charakterisierung der gasförmigen Emissionen aus LIB während des Schadensfalls entwickelt. Dies wurde durch die Kombination der analytischen Fähigkeiten von Gaschromatographie/Massenspektrometrie (GC/MS) und Fourier-Transform Infrarotspektroskopie (FTIR) ermöglicht. Ein Messplatz wurde aufgebaut, an dem die freigesetzten Gase durch simultane Messung via GC/MS und FTIR kontinuierlich erfasst werden können. GC/MS ermöglicht die Identifizierung und Quantifizierung der Analyte während FTIR rasche Konzentrationsänderungen mit hoher Zeitauflösung detektiert. Mittels einer *partial-least-squares* Regression wurden die GC/MS Daten mit dem FTIR-Signal korreliert. Diese Methode

wurde erfolgreich zur Charakterisierung der Gasentwicklung in Knopfzellen und kommerziellen High-Power-Batterien eingesetzt.

Die flüchtigen Zersetzungsprodukte einer kommerziellen Zelle während eines kontrollierten Überlade-Programms wurden identifiziert und ihre Entwicklung relativ zur Ladenspannung beobachtet. Weiters wurden die entwickelten Gase aus mehreren Elektrolytmischungen während eines Cyclovoltammetrie-Experiments identifiziert und die Stabilität der Elektrolyt-Bestandteile charakterisiert. Der Einfluss des Elektrodenmaterials auf das Produktspektrum und das Zersetzungsverhalten wurde an einer inerten Arbeitselektrode und einer realen Batteriekathode untersucht. Ein besonderes Augenmerk galt der Entwicklung und Beurteilung der neuen Methode.

## Appendix D

# Curriculum Vitae

Alfred Amon

06/2007	Matura, <i>Gymnasium d. Herz-Jesu Missionare</i> , Salzburg, Austria
2008 – 2011	Bachelor's course <i>Chemistry</i> , University of Vienna, Austria
06/2011	Bachelor's thesis, Institute of Materials Chemistry, University of Vienna, Austria. Supervisor: Prof. Klaus Richter. <i>Investigation of Ti-Al-Ge alloys for High-Temperature Soldering</i>
10/2011 – 09/2014	Master's Course <i>Chemistry and Technology of Materials</i> , TU Vienna and University of Vienna
10/2013 – 05/2014	Master's thesis, Austrian Institute of Technology, Vienna, Austria. Supervisor: Prof. Erwin Rosenberg (TU Vienna), Co-Supervisor: Prof. Atanaska Trifonova (AIT). <i>Gas evolution from Lithium ion batteries studied in-situ by coupled GC/MS-FTIR</i>